Stiffness and Strength Predictions of Discontinuous Fiber Composites

Karen Harban

A thesis

Submitted in partial fulfillment of the

Requirements for the degree of

Master of Science in Engineering

University of Washington

2015

Committee:

Mark Tuttle

Ramulu Mamidala

Nathan Sniadecki

Program Authorized to Offer Degree:

Mechanical Engineering

University of Washington

Abstract

Stiffness and Strength Predictions of Discontinuous Fiber Composites

Karen Harban

Chair of the Supervisory Committee:
Dr. Mark Tuttle
Mechanical Engineering Department

The overall goal of this study is to develop a numerical modeling approach that will ultimately lead to the certification of discontinuous fiber composites based on analysis and modest experimental verification. A discontinuous fiber composite (DFC) material system called HexMC is considered in this study. A stochastic (Monte Carlo-type) finite-element modeling approach called the Stochastic Laminate Analogy has been developed. During a typical analysis the DFC structure of interest is divided into regions called Random Laminate Volume Elements (RLVEs). A unique randomly-generated and non-symmetric stacking sequence is assigned to each RLVE. Experimentally-observed variations in the stiffness of a DFC part are then simulated by performing many FE analyses, where a new random stacking sequence is generated for each RLVE during each analysis. Fracture predictions are obtained through a damage accumulation model called the ply discount scheme. Final structural failure of the part is declared when all plies within a single element have failed. Other definitions of final structural failure are also explored in this study. A typical analysis predicts that ply failures (i.e., “damage”) will evolve in a distributed manner throughout a typical DFC structure, even in the presence of stress risers. This damage pattern is in qualitative agreement with experimental observation. Analyses of un-notched and notched tension

coupon specimens are discussed in this paper, and predicted B-basis and B-Max measures of modulus and strengths are presented.

TABLE OF CONTENTS

List of Figures 1

List of Tables 3

Chapter 1. Introduction 6

1.1 Problem statement 8

1.2 Objective 9

Chapter 2. LITERATURE REVIEW 10

2.1 Hexmc Properties 10

2.2 Analysis Techniques For Discontinuous Fiber Composites 10

2.3 Sheet Molding Compound 11

Chapter 3. stochastic laminate analogy 11

3.1 Nominal Dimensions 12

3.1.1 Un-notched Tension 12

3.1.2 Notched Tension 14

3.2 Random Layup Volume Element 16

3.3 Modeling 17

3.3.1 Finite Element Modeling 17

3.3.2 Boundary/Loading Conditions 18

3.3.3 Mesh Study 19

3.3.4 Quasi – Isotropic Material Properties 26

Chapter 4. STIFFNESS PREDICTIONS BASED ON SLA 28

4.1 B-max and B-basis Definitions 29

4.2 B-max and B-basis Calculations 30

4.2.1 Sample Mean and Standard Deviation 31

4.2.2 Outliers 33

4.2.3 Normal Distribution 33
4.2.4 Coefficient of Variance 34
4.2.5 B-Basis and B-Max Tolerance Factor 36
4.2.6 B-Basis and B-Max Values 37
4.3 B-max and B-basis Results 39
Chapter 5. STRENGTH PREDICTIONS BASED ON SLA 43
5.1 Modeling 43
5.1.1 Material Properties 44
5.1.2 Final Structural Failure 45
5.2 Tsai – Wu Failure Criteria 46
5.2.1 HexMC Failure Strengths 47
5.2.2 Tsai – Wu Constants 49
5.3 Strength Results 50
5.3.1 First Structural Failure Criteria of Un-notched 51
5.3.2 First Structural Failure Criteria of Notched 58
5.3.3 Discussion of First Structural Failure 67
5.3.4 Second Structural Failure Criteria of Notched 69
5.3.5 Second Structural Failure Discussion 71
Chapter 6. Experimental TESTING 72
6.1 Measured Dimensions 72
6.2 Experiment Setup 74
6.3 Experimental Results 75
6.4 Improvement Of Predictions 77
Chapter 7. CONCLUSION 79
Chapter 8. FUTURE WORK 80
REFERENCES 81

LIST OF FIGURES

Figure 1.1. Images illustrating the chip structures of HexMC [3]. 6
Figure 3.1. RLVEs of un-notched tension specimen. 15
Figure 3.2. RLVEs of notched tension specimen. 15
Figure 3.3. Boundary/loading conditions of un-notched tension specimen..... 17
Figure 3.4. Boundary/loading conditions of notched tension specimen 17
Figure 3.5. Von Mises Stress contour plot of un-notched tension specimen..... 18
Figure 3.6. Von Mises Stress contour plot of notched tension specimen 19
Figure 3.7. Finite element of selected mesh size of an un-notched specimen 19
Figure 3.8. Resulting Von Mises Stress of notched diameter 3.18 mm (0.125 in)..... 20
Figure 3.9. Resulting Von Mises Stress of notched diameter 6.35 mm (0.25 in)..... 20
Figure 3.10. Resulting Von Mises Stress of notched diameter 9.53 mm (0.375 in)..... 20
Figure 3.11. Resulting Von Mises Stress of notched diameter 12.7 mm (0.05 in)..... 21
Figure 3.12. Max Von Mises Stress of bottom ply for different notch diameters 22
Figure 3.13. Mesh of notch diameter 3.18 mm (0.125 in) 22
Figure 3.14. Mesh of notch diameter 6.35 mm (0.25 in) 23
Figure 3.15. Mesh of notch diameter 9.53 mm (0.375 in) 23
Figure 3.16. Mesh of notch diameter 12.7 mm (0.50 in) 23
Figure 4.1. Resulting axial fores of a typical un-notched specimen 27
Figure 4.2. Normal probablity function of stiffness data 32
Figure 4.3. B-max, average and B-basis stiffness values for un-notched specimen..... 39
Figure 4.4. Comparison between predicted and measured tensile moduli 40
Figure 5.1. Flow chart of the Ply Discount Scheme 41
Figure 5.2. Flow chart of the Ply Discount Scheme implementing the first final structural failure condition 43
Figure 5.3. Chip Failure distribution of un-notched specimen thickness of 1.02 mm (0.04 in) 50

Figure 5.4. Chip Failure distribution of un-notched specimen thickness of 4.06 mm (0.16 in) 50
Figure 5.5. Strength versus strain curves for UNT of 1.02 mm (0.04 in) thick..... 51
Figure 5.6. Strength versus strain curves for UNT of 4.06 mm (0.16 in) thick..... 51
Figure 5.7. B-max, average and B-basis strength values for UNT specimen..... 52
Figure 5.8. Normal Distribution of 1.02 mm (0.04 in) thick specimen. 56
Figure 5.9. Normal Distribution of 4.06 mm (0.16 in) thick specimen. 56
Figure 5.10. Representative gross strength-strain curves for notch diameter 3.18 mm (0.125 in) 61
Figure 5.11. Representative gross strength-strain curves for notch diameter 6.35 mm (0.25 in) 62
Figure 5.12. Representative gross strength-strain curves for notch diameter 9.53 mm (0.375 in) 62
Figure 5.13. Representative gross strength-strain curves for notch diameter 12.7 mm (0.50 in) 63
Figure 5.14. Distribution of chip failure for notch diameter 3.18 mm (0.125 in)..... 63
Figure 5.15. Distribution of chip failure for notch diameter 6.35 mm (0.25 in)..... 64
Figure 5.16. Distribution of chip failure for notch diameter 9.53 mm (0.375 in)..... 64
Figure 5.17. Distribution of chip failure for notch diameter 12.70 mm (0.50 in)..... 65
Figure 5.18. Variation of notched strength using gross-sectional area..... 65
Figure 5.19. B-basis, average and B-max gross strengths for notch specimens..... 66
Figure 5.20. Strength-strain curve when 2,000 chips failed 67
Figure 5.21. Strength-strain curve when 10,000 chips failed 67
Figure 6.1. Experimental setup using Instron 5585H 75
Figure 6.2. Fracture regions of HexMC flat panels 76
Figure 6.3. Stress versus strain for five HexMC flat panels 77

LIST OF TABLES

Table 2.1. Nominal HexMC Elastic Properties [6] 8
Table 2.2. Nominal HexMC Strength Values [6] 8
Table 3.1. Un-notched tension dimensions 11
Table 3.2. Actual Dimensions of un-notched specimens 12
Table 3.3. Notched tension dimensions 13
Table 3.4. Actual Dimensions of notched specimens 14
Table 3.5. Properties for AS4/8552 Graphite – Epoxy at Room Temperature [14] 24
Table 3.6. Properties for HexMC at Room Temperature [15] 25
Table 3.7. Material Properties used in this study 25
Table 4.1. Sample mean and standard deviation 30
Table 4.2. Coefficient of Variances 33
Table 4.3. B-basis, average and B-max stiffness values 38
Table 5.1. Material Properties used in the ply discount scheme 42
Table 5.2. Failure Strengths of AS4/8552 Graphite Epoxy uni-directional Prepreg 45
Table 5.3. Failure Strengths used in this study 45
Table 5.4. New Failure Strengths used on failed chips 46
Table 5.5. Tsai-Wu constants used in this study 47
Table 5.6. Strength Results for two un-notched specimen thickness 48
Table 5.7. B-basis, Average and B-max Strength values for un-notched specimens 48
Table 5.8. Strength Results for notch diameter of 3.18 mm (0.125 in) 58
Table 5.9. Strength Results for notch diameter of 6.35 mm (0.25 in) 59

Table 5.10. Strength Results for notch diameter of 9.53 mm (0.375 in) 59
Table 5.11. Strength Results for notch diameter of 12.7 mm (0.50 in) 60
Table 5.12. B-max, B-basis and average values of notched specimens 65
Table 5.13. Strength values when 2,000 chips fail 67
Table 5.14. Strength values when 10,000 chips fail 67
Table 6.1. Width and thickness dimensions of four different locations 73
Table 6.2. Nominal width and thickness dimensions 74

ACKNOWLEDGEMENTS

I wish to thank my advisor, Dr. Mark Tuttle for presenting the opportunity to be a part of this project and for assisting and supporting me through my Masters research. I would like to extend my gratitude to Bruno Boursier, and Sanjay Sharma from Hexcel, Larry Ilcewicz from FAA, and Bill Avery from Boeing for providing technical guidance and funding for this research. I would like to thank previous graduate students Tory Shiffman, Brian Head and Michael Arce who laid the groundwork for the research presented herein.

Chapter 1. INTRODUCTION

Composite materials consist of two or more materials (reinforcing elements and matrix material) that are bonded together at the atomic/molecular level. The high strength to weight ratios and high stiffness to weight ratios exhibited by composites enhances the use of composites in aircraft structures, automotive parts and even in communication devices. Composites are widely utilized in a spectrum of applications, especially the aerospace and automotive industry. A breakthrough in the field of composites is evidenced by the Boeing 787 Dreamliner, which has 50% of its airframe made out of composites [1, 2].

Both continuous fiber composites and discontinuous fiber composites are used in modern aircraft. Continuous fiber composites are based on very long fibers, i.e., fibers that are long enough to be considered "continuous". Continuous fiber composites are used to produce multi-ply laminated structures, where fiber angles vary from one ply to the next. The number of plies and ply fiber angles, collectively called the "stacking sequence" of the laminate, can be selected to achieve the desired directional strength and stiffness. Continuous fiber composites have very high strength- and stiffness-to-weight ratios, and are used extensively in critical load-bearing aircraft structures. In contrast, relatively short fibers are used in discontinuous fiber composite (DFC) material systems. In these types of composites the fiber length is typically on the order of 0.1cm - 10 cm (0.4 in – 4 in). A widely-used DFC is known as "sheet molding compound", which usually consists of randomly oriented glass fibers embedded within a polyester matrix. DFCs can be used to produce relatively inexpensive and complex shapes using injection molding

or compression molding. Sheet molding compounds have long been used to produce household goods or appliances for example.

DFCs possess low strength- and stiffness-to-weight ratios when compared to their continuous-fiber composites. For this reason DFCs have not been widely used in the past for critical load-bearing aircraft structures. However, a new generation of DFCs has been developed that consist of randomly oriented chips of B-staged graphite-epoxy pre-preg-rather than individual randomly-oriented fibers. These new materials have improved stiffness- and strength-to weight ratios and are currently being used in commercial transport aircraft. For example, load-bearing parts produced using a DFC called HexMC are used on the Boeing 787.

HexMC is produced using chipped B-staged AS4/8552R graphite epoxy unidirectional pre-preg that is slit, chopped and randomly deposited on a release backing, forming a pre-preg layer. Nominal chip dimensions are 0.15 mm x 7.6 mm x 50 mm (0.006 in x 0.30 in x 2 in). HexMC parts are produced using compression molding. The randomly-oriented chips can be readily seen on an external surface of a HexMC part, as shown in Figure 1.1a [3]. Micrographs of typical through-thickness chip structure are presented in Figure 1.1b,c. Together these images show that HexMC parts can be roughly visualized as a laminated composite part in which the local stacking sequence (as represented by the local through-thickness chip structure) varies continuously throughout the part. Discontinuous fibers are used in certain load bearing structures as they are relatively easy to manufacture complex parts with fast curing times, have near quasi-isotropic in-plane stiffness and strengths [4] and have a high delamination resistance.

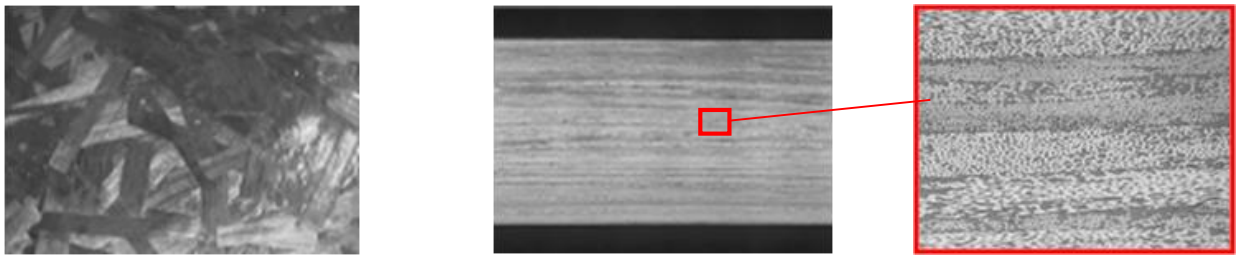

(a) Typical surface of a HexMC part, showing random orientation of AS4/8552 chips

(b) Edge view of a HexMC part

(c) Magnified edge view of a HexMC part, showing roughly laminar through-thickness chip structure

Figure 1.1 Images illustrating the chip structure of HexMC [3].

1.1 PROBLEM STATEMENT

Although next-generation DFCs such as HexMC provide many advantages, there are significant disadvantages as well. These include a high level of scatter in DFC stiffness and strength properties and notch insensitivity, as compared to continuous-fiber composites [5]. . Consequently it is difficult to perform structural analyses of HexMC parts with a high level of confidence. Since analytical predictions are viewed with a high level of skepticism, in practice the certification of DFC aircraft parts are achieved through extensive experimental testing. This is a time consuming and very costly approach, and probably leads to over-conservative part designs. Analytical and/or numerical methods capable of accurately predicting the stiffness and strength of DFC parts are sorely needed by the aircraft industry. If suitable analysis procedures are developed, then a new far less costly certification process based on analysis supplemented by relatively modest experimental measurements will emerge.

1.2 OBJECTIVE

The overall goal of this study is to help establish methods to certify prepreg-based DFC aircraft parts. Towards that end, a stochastic (Monte Carlo-type) finite element modeling approach called the Stochastic Laminate Analogy has been previously developed at the UW [Head, Arce]. This approach will be applied to the HexMC material system during this study. Specific tasks are:

1. Use the Stochastic Laminate Analogy to predict B-basis and B-Max tensile moduli for simple HexMC tensile coupons
2. Develop a practical failure criterion coupled with the Stochastic Lamiante Analogy and suitable for use with HexMC structures.
3. Predict the B-basis and B-Max allowable tensile strengths for unnotched and notched HexMC tensile coupons.

Chapter 2. LITERATURE REVIEW

2.1 HEXMC PROPERTIES

The properties of HexMC used in commercial aircraft like the Boeing 787 are proprietary. Hence, the properties used in this study were obtained from the unidirectional AS4/8552 material system. Table 2.1 lists the nominal in-plane modulus values and Table 2.2 lists strength values of AS4/8552 material system [14].

Table 2.1. Elastic Properties for unidirectional AS4/8552 [14].

E_{11}	E_{22}	G_{12}	ν_{12}
131.7 GPa (19.1 Msi)	9.238 GPa (1.34 Msi)	4.83 GPa (0.7 Msi)	0.302

Table 2.1 Strength values for unidirectional AS4/8552 [14].

0^0 Strength		90^0 Strength		In-plane Shear Strength
Tensile	Compression	Tensile	Compression	
2.061 GPa (299 ksi)	1.48 GPa (215 ksi)	63.91 MPa (9.27 ksi)	265.6 MPa (38.38 ksi)	91.55 MPa (13.28 ksi)

2.2 ANALYSIS TECHNIQUES FOR DISCONTINUOUS FIBER COMPOSITES

Previous work on predicting the behavior of short fiber composites has been reported. Halpin and Pagano developed a laminate analogy to predict the strength and stiffness of short fiber composites in early 1968 [3]. This laminate analogy was later modified by Feraboli and

colleagues [8]. This study's objective is to predict the strength and stiffness of discontinuous fiber composites based on the stochastic laminate analogy adopted by Brian Head and Michael Arce [9]. Section 3 describes in detail the basis of the laminate analogy proposed by Halpin, Pagano and Feraboli and the modification made to implement the laminate analogy in this study.

2.3 SHEET MOLDING COMPOUND

Two common short fiber composite materials are known as sheet molding compound and bulk molding compound. Sheet molding compounds (SMCs) are typically used with compression molding processes. Bulk molding compounds on the other hand, are used in injection molding processes and provide a very high dimensional tolerance [10]. Typical sheet molding compounds that are compression molded feature 25.4 mm (1in) long glass fibers and less than about 40% epoxy resin content by volume. These traditional sheet molding compound material forms have lower mechanical properties and may be undesirable for secondary aircraft structures [11]. In order to fulfill the desirability of sheet molding compounds in secondary aircraft structures, a higher performance sheet molding compounds were created. An example of a commercial application for this higher performance sheet molding compound is the HexMC produced by Hexcel. Higher performance sheet molding compounds are produced through compression molding of chopped uni-directional pre-preg. This study predicts the strength and stiffness of HexMC, a high performance sheet molding compound material system.

Chapter 3. STOCHASTIC LAMINATE ANALOGY

The stochastic laminate analogy is a modeling approach that accounts for variation in chip orientation through the thickness of the material developed at the UW. A probabilistic modeling

approach was suggested by Feraboli et al. [7], and was considered an extension of earlier work by Halpin and Pagano [8]. That modeling approach showed that the laminate analogy was successful in capturing local variations in elastic modulus in discontinuous fiber composite parts. A limitation of Feraboli's initial laminate analogy was the assumption of a symmetric stacking sequence with uniform increments between orientations of ply. This condition does not adequately represent the randomly distributed chips present in HexMC parts. Further modifications were made to the approach called the stochastic laminate analogy by Head and Tuttle [9], and was implemented in finite-element analyses. In contrast with Feraboli's stochastic laminate analogy, Head adapted the stochastic laminate analogy approach that accounts for a random, non-symmetric stacking sequence through the thickness. This approach accounts for the possibility of membrane-bending coupling effects and the resulting out-of-plane displacements due to in - plane loading. The stochastic laminate analogy used in this study proceeds by first dividing the HexMC structure to be modeled into regions called the Random Laminate Volume Element (RLVE). A random, non-symmetric stacking sequence is assigned to each RLVE, which is further divided into finite element meshes and the use of laminate shell elements and designated material properties to obtain elastic modulus properties.

3.1 NOMINAL DIMENSIONS

3.1.1 *Un-notched Tension*

To begin the stochastic laminate analogy, dimensions reported by HexMC Design Allowable Test Plan [12] were used, with modifications made to specimen thickness. Table 3.1 lists the dimensions of un-notched tension specimens for AS4/8552R material system.

Table 3.1. Un-notched Tension Dimensions from TP 1031-SW

Test Type	Target thickness	Width	Length
Un-notched Tension	2.3 mm (0.090 in)	38.1 mm (1.5 in)	305 mm (12 in)
	3.6 mm (0.140 in)	38.1 mm (1.5 in)	305 mm (12 in)
	5.8 mm (0.023 in)	38.1 mm (1.5 in)	305 mm (12 in)
	9.4 mm (0.037 in)	38.1 mm (1.5 in)	305 mm (12 in)

The actual thickness values used in this study were adjusted to study the stiffness variation for different ply thickness and to account for a reduction in analysis time. Table 3.2 lists the actual dimensions for un-notched tension specimens used in this study.

Table 3.2. Actual Dimensions of Un-notched Tension Specimens

Test Type	Target thickness	Width	Length
Un-notched Tension	1.02 mm (0.040 in)	38.1 mm (1.5 in)	305 mm (12 in)
	2.03 mm (0.080 in)	38.1 mm (1.5 in)	305 mm (12 in)
	2.30 mm (0.090 in)	38.1 mm (1.5 in)	305 mm (12 in)
	3.05 mm (0.120 in)	38.1 mm (1.5 in)	305 mm (12 in)
	4.06 mm (0.160 in)	38.1 mm (1.5 in)	305 mm (12 in)
	5.80 mm (0.23 in)	38.1 mm (1.5 in)	305 mm (12 in)
	9.40 mm (0.37 in)	38.1 mm (1.5 in)	305 mm (12 in)

3.1.2 *Notched Tension*

The notched tension dimensions obtained from HexMC Design Allowable Test Plan [8] were used for this study, with two additional notch diameters. Table 3 lists the dimension of notched tension specimens reported by the test plan. An additional notch diameter dimension were added to the dimensions listed in Table 3.3 to have a set of dimensions comparable to the notch diameter dimensions used in Feraboli's report [4]. The same length and width dimensions were used, 305 mm (12 in) by 38.1 mm (1.5 in). Table 3.4 lists the actual notch diameter and thickness dimensions used for this study. Previous work done by Feraboli [5] showed that the variation in strength for various un-notched specimen thickness were about 8% - 16% difference. Since the differences in strength relative to the thickness are small, the thickness variation for notched specimens were neglected. Instead, variation of notched strength with hole diameter was the focus of Feraboli's study on behavior of notched pre-preg based discontinuous fiber systems [5]. Another literature reported that most prior studies conducted on notched behavior of discontinuous fiber composites focused on constant hole-to-width ratio and constant width relations, without any consideration for the specimen size effects which includes thickness [22]. Hence, from the findings of the two literature mentioned, this study focused only on the effects of notch diameter on the strength behavior.

Table 3.3. Notched Tension Dimensions from TP 1031-SW

Test Type	Target thickness	Width	Length	Hole Diameter
Notched Tension	2.3 mm (0.090 in)	38.1 mm (1.5 in)	305 mm (12 in)	6.35 mm (0.250 in)
	3.6 mm (0.140 in)	38.1 mm (1.5 in)	305 mm (12 in)	6.35 mm (0.250 in)
	5.8 mm (0.023 in)	38.1 mm (1.5 in)	305 mm (12 in)	6.35 mm (0.250 in)
	9.4 mm (0.037 in)	38.1 mm (1.5 in)	305 mm (12 in)	6.35 mm (0.250 in)
	2.3 mm (0.090 in)	38.1 mm (1.5 in)	305 mm (12 in)	9.53 mm (0.375 in)
	3.6 mm (0.140 in)	38.1 mm (1.5 in)	305 mm (12 in)	9.53 mm (0.375 in)
	5.8 mm (0.023 in)	38.1 mm (1.5 in)	305 mm (12 in)	9.53 mm (0.375 in)
	9.4 mm (0.037 in)	38.1 mm (1.5 in)	305 mm (12 in)	9.53 mm (0.375 in)

Table 3.4. Actual Dimensions of Notched Tension Specimens

Test Type	Thickness	Hole Diameter			
Notched Tension	2.3 mm (0.090 in)	3.18 mm (0.125 in)	6.35 mm (0.125 in)	9.53 mm (0.375 in)	12.7 mm (0.50 in)

3.2 RANDOM LAYUP VOLUME ELEMENT

Random Layup Volume Element (RLVEs) are discretized regions of a modeled HexMC structure. RLVE sizing was determined by monitoring the effective elastic properties over a large number of coupon level finite element analyses. The size that resulted in the smallest deviation across those analyses which was a square nominally 19.30 mm (0.76 in) on a side [12]. The RLVEs in the notched and un-notched models with length of 305 mm (12 in) were of length and width dimensions 19.05 mm (0.75 in). The idea was to discretize the model into 32 RLVE squares with equal length and width dimensions. Figure 3.1 shows the random layup volume element for an un-notched specimen of dimensions 38.1 mm (1.5 in) by 305 mm (12 in). Figure 3.2 shows the random layup volume element for a notched specimen with a notch diameter of 12.7 mm (0.50 in). The ply orientation in one RLVE is unique and differs from the neighboring RLVEs. This condition simulates the random, non-symmetric stacking sequence present in discontinuous fiber composites. A Visual Basic code was written to generate a vector of random angles ranging from 0 to 180 degrees, which is assigned to a RLVE. Each RLVE has a unique vector of angles and the size of the

vector depends on the thickness of the specimen. For instance, a 1.02 mm (0.040 in) thick specimen corresponds to 8 through-thickness chips which results in a random angle column vector of size 8.

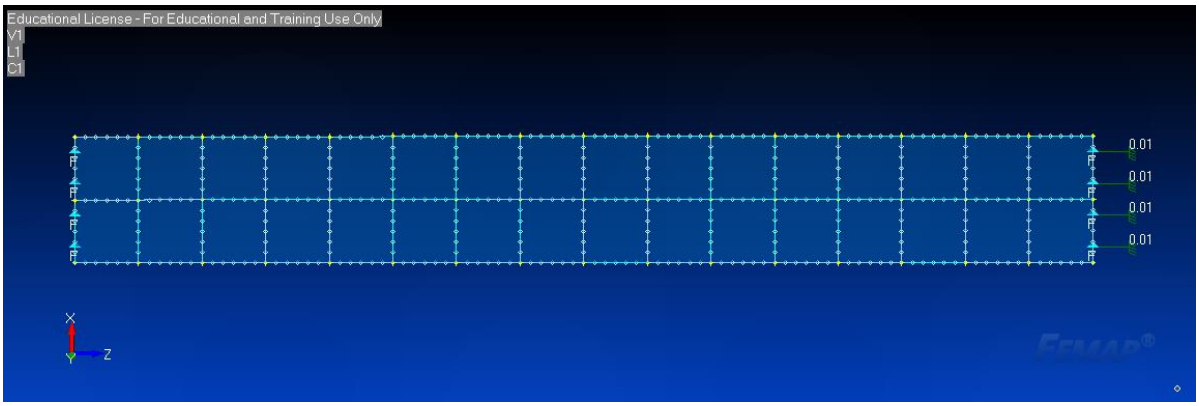

Figure 3.1. RLVEs of an un-notched specimen.

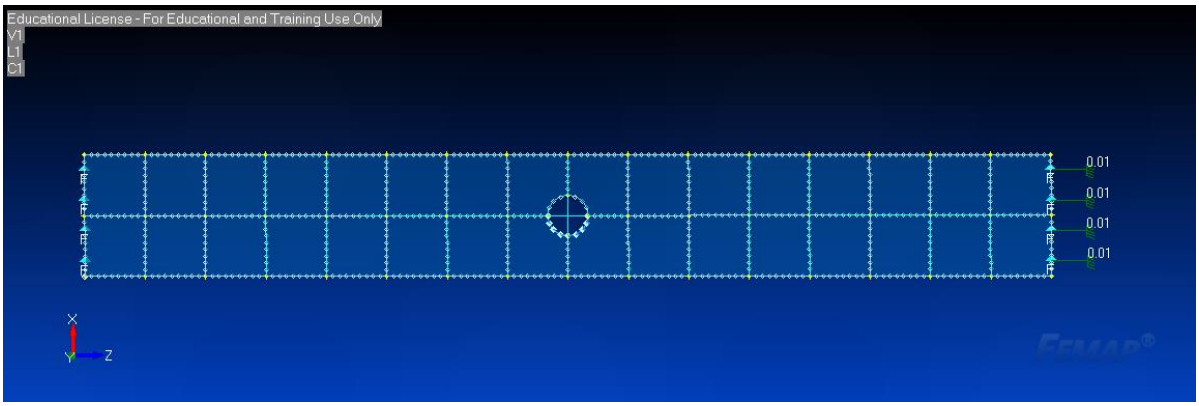

Figure 3.2. RLVEs of notched specimen.

3.3 MODELING

3.3.1 *Finite Element Modeling*

The un-notched and notched specimens were modeled using SolidWorks and imported into FEMAP. Solidworks is a 3D computer aided-design software, while FEMAP is a commercial pre

and post processor. FEMAP is integrated in the NX NASTRAN finite element solver. NX Nastran is an industry standard finite element solver for stress, structural failure, heat transfer, acoustics and aeroelasticity. Finite element modeling was divided into two stages; the pre-processing stage and the post-processing stage. In the pre-processing stage, a mid-surface model of the HexMC structure was first created and discretized into 32 RLVEs. A mesh was then created to discretize the model into finite elements ranging from 1152 to 3868 elements, resulting in a number of nodes ranging from 1261 to 4042 depending on the presence of a notch and the mesh size.

The number of elements in an RLVE were non-uniform for the notched specimens as compared to the un-notched specimens; there were fewer elements in an RLVE in regions closer to the notch. Laminate shell elements were used with 2D orthotropic properties. The appropriate boundary/loading conditions were applied. In the post-processing stage, the models were analyzed using NX Nastran's Linear Static Analysis Solution. The linear static analysis represents a linearly related computed response – displacement or stress, to the time independent applied force. NX Nastran is based on the displacement method where the equations of motion are written with displacements as the unknown. For each loading and boundary condition set specified in the pre-processing stage, a stiffness solution is performed. Once the displacements are computed, NX Nastran uses these stiffness matrices to compute element forces, stresses or forces, and strains [13].

3.3.2 *Boundary/Loading Conditions*

The boundary and loading conditions applied to the tensile un-notched and notched specimens simulates the loading and constraints used during testing in the HexMC Design Allowable Test Plan [12]. An enforced displacement was applied to the top edge of the specimens and the bottom

edges fixed. Figures 3.3 and 3.4 shows the boundary/loading condition applied to an un-notched and notched specimen.

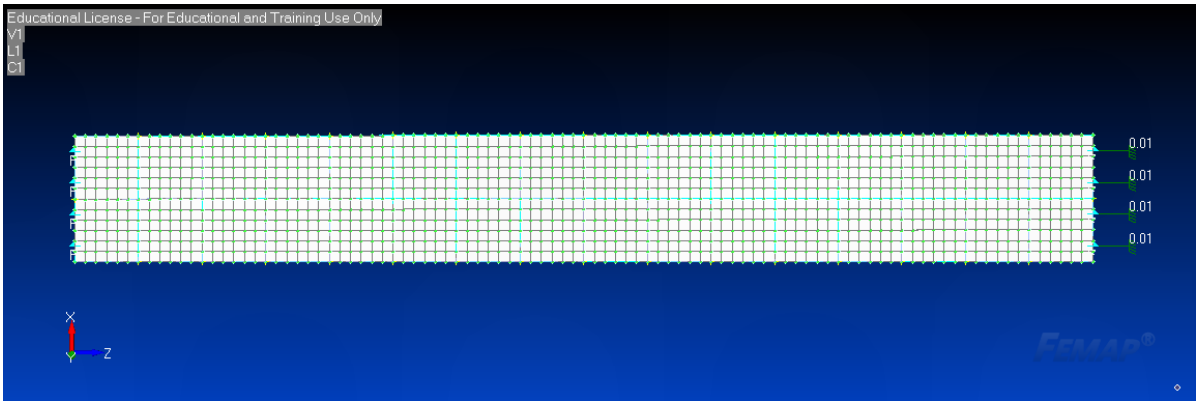

Figure 3.3. Boundary/loading condition for un-notched tension specimen.

.

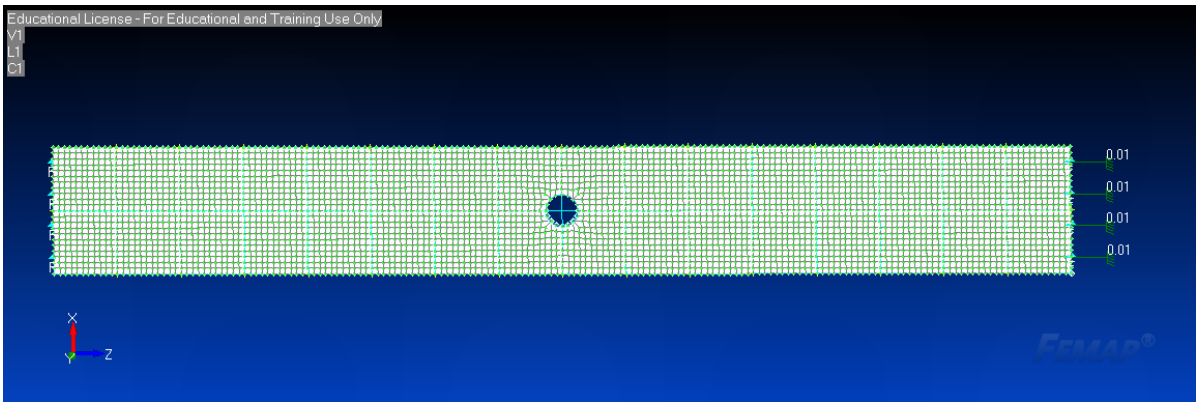

Figure 3.4. Boundary/loading condition for notched tension specimen

3.3.3 *Mesh Study*

A mesh study was performed to decide the appropriate mesh size for the un-notched and notched specimens. An enforced unit displacement of 0.254 mm (0.01in) was applied to the top edge and the resulting maximum von Misses stresses were obtained. Figure 3.5 shows a contour plot of the resulting Von Misses stress in the bottom ply for the un-notched specimen. Figure 4 shows a plot

of maximum von Misses stress for the bottom ply against the mesh size for un-notched specimens with dimensions of 38.1 mm (1.5 in) and 305 mm (12 in). The mesh study is irrelevant of the panel thickness, since a mid-surface model concerns only the length and width dimensions. The mesh sizes for un-notched panels which ranged from 2.03 mm (0.08 in) to 4.06mm (0.16 in) showed no distinct convergence pattern. The chosen mesh size for un-notched specimens in this finite element modeling process was 3.05 mm (0.12 in) which was the default mesh size in FEMAP Nastran. Figure 3.6 shows a plot of the maximum Von Mises stress of the bottom ply for the different mesh sizes for an un-notched specimen.. Figure 3.7 shows the chosen mesh size for the un-notched specimen.

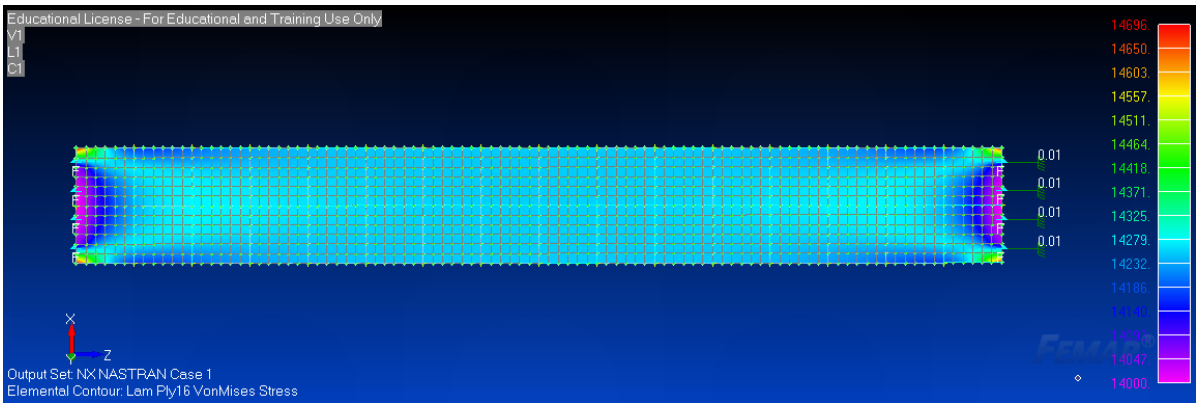

Figure 3.5. Von Mises stress contour plot for an un-notched specimen

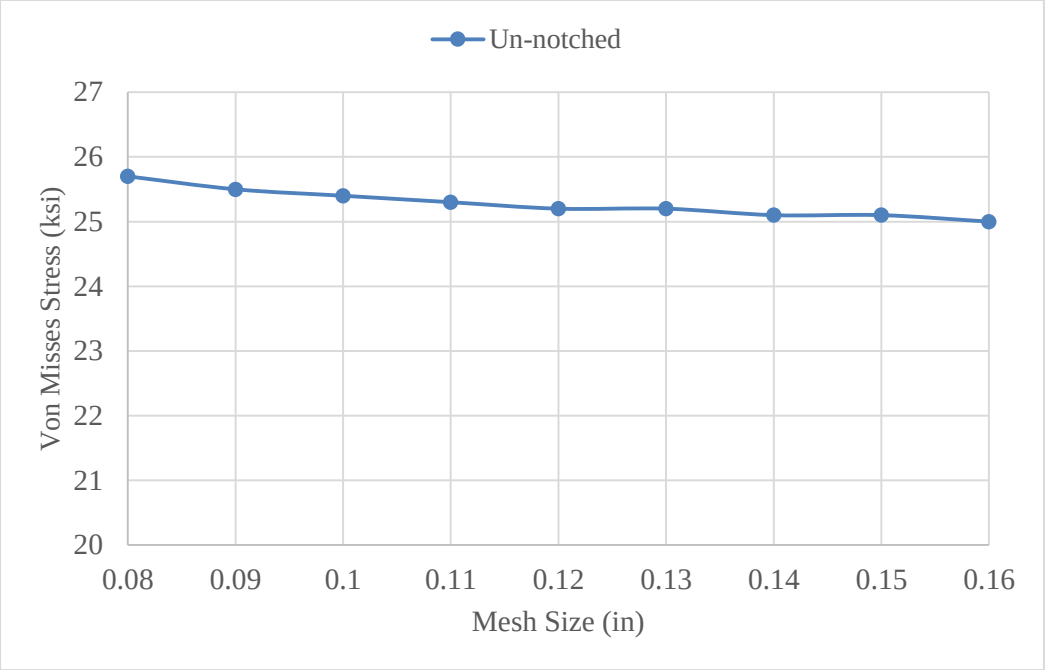

Figure 3.6. Maximum Von Mises Stress of bottom ply for an un-notched specimen.

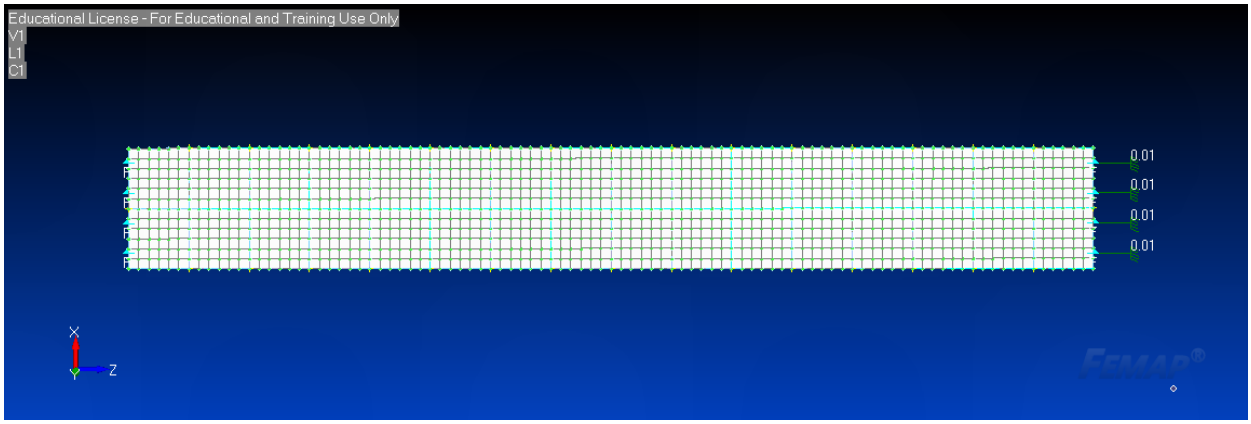

Figure 3.7. Finite element of selected mesh size of an un-notched specimen.

The mesh sizes for notched specimens were between the range of 1.27 mm (0.05 in) and 3.3 mm (0.13 in). Figure 9 shows a plot of the maximum Von Mises stresses against the different mesh sizes for notch diameters of 3.18 mm (0.125 in), 6.35 mm (0.25 in), 9.53 mm (0.375 in) and 12.7 mm (0.50 in). Figures 3.8 to 3.11 shows a contour plot of the maximum Von Mises stress for the bottom ply of the notched models.

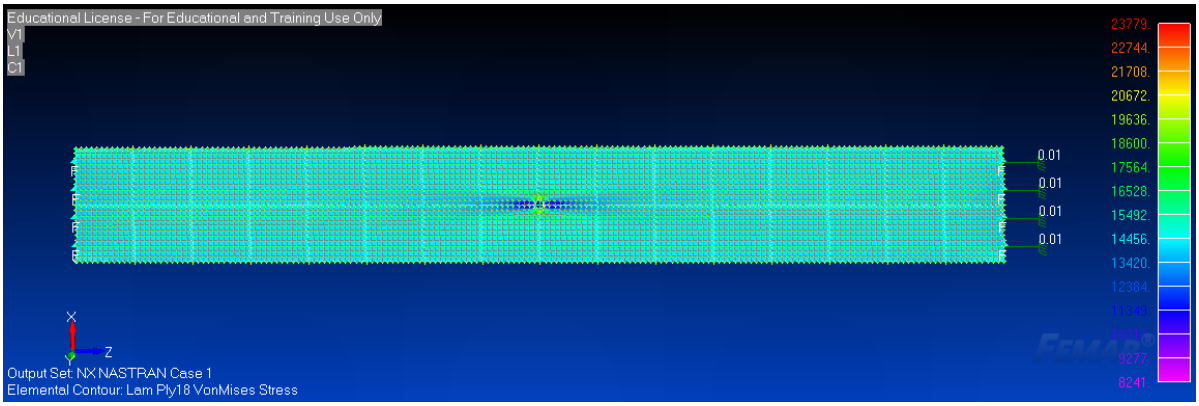

Figure 3.8. Resulting Von Mises Stress of notch diameter 3.18 mm (0.125 in).

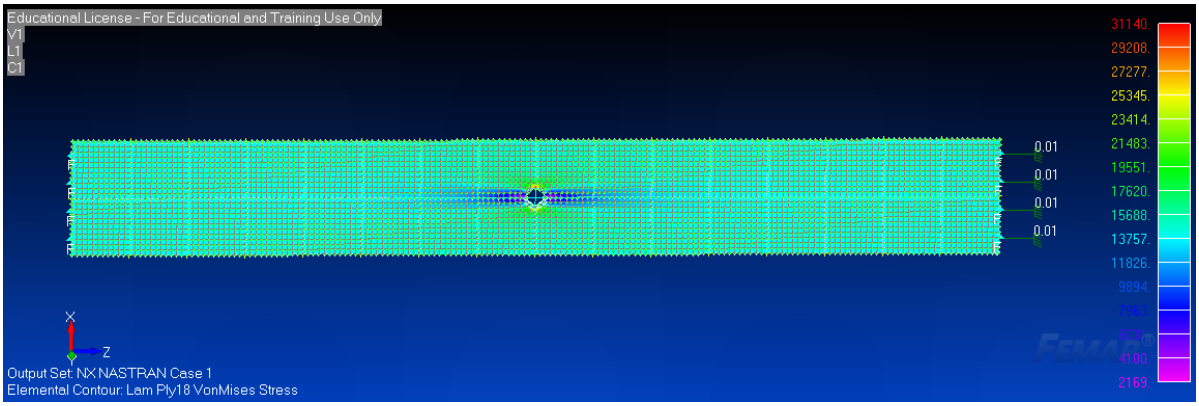

Figure 3.9. Resulting Von Mises Stress of notch diameter 6.35 mm (0.25 in).

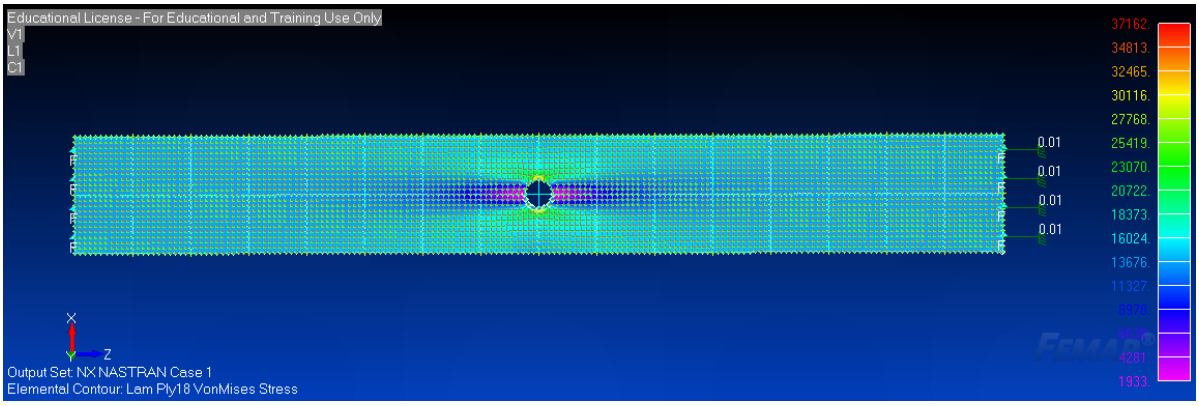

Figure 3.10. Resulting Von Mises Stress of notch diameter 9.53 mm (0.375 in).

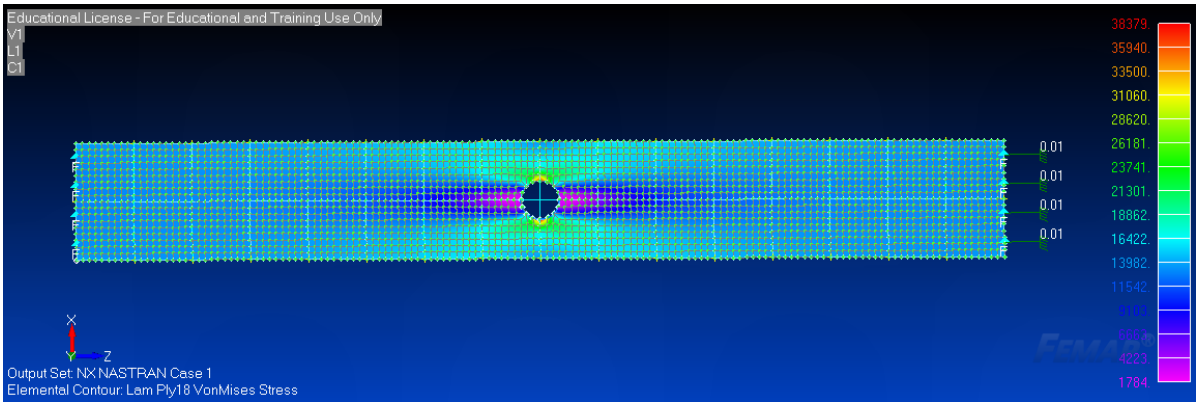

Figure 3.11. Resulting Von Mises Stress of notch diameter 12.7 mm (0.50 in).

The number of elements and nodes that are generated are greatly increased as a finer mesh size is used which leads to longer computation times. Hence, a mesh size that generated a reasonable number of elements, nodes, and that had all quad elements was selected. A uniform mesh size throughout the entire specimen region for both notched and un-notched specimens was used. Figure 3.12 shows a plot of Von Mises Stress for each notch diameter. For notch specimens, a finer mesh around the notch region would induce high stress regions near the notch and would enforce chip failure in that region. Hence, to eliminate the possibility of inducing chip failure near that region, a uniform mesh size was used. Figures 3.13 to 3.16 shows the finite element mesh size chosen for different notch diameters. The mesh size selected for notched specimens with diameters 3.18 mm (0.125 in), 6.35 mm (0.25 in) and 9.53 mm (0.375 in) was 1.78 mm (0.07 in). The notched specimen with the largest diameter, 12.7 mm (0.50 in) on the other hand, had a mesh size of 2.54 mm (0.10 in) with consideration of the number of elements, nodes, use of only quad elements and computation time.

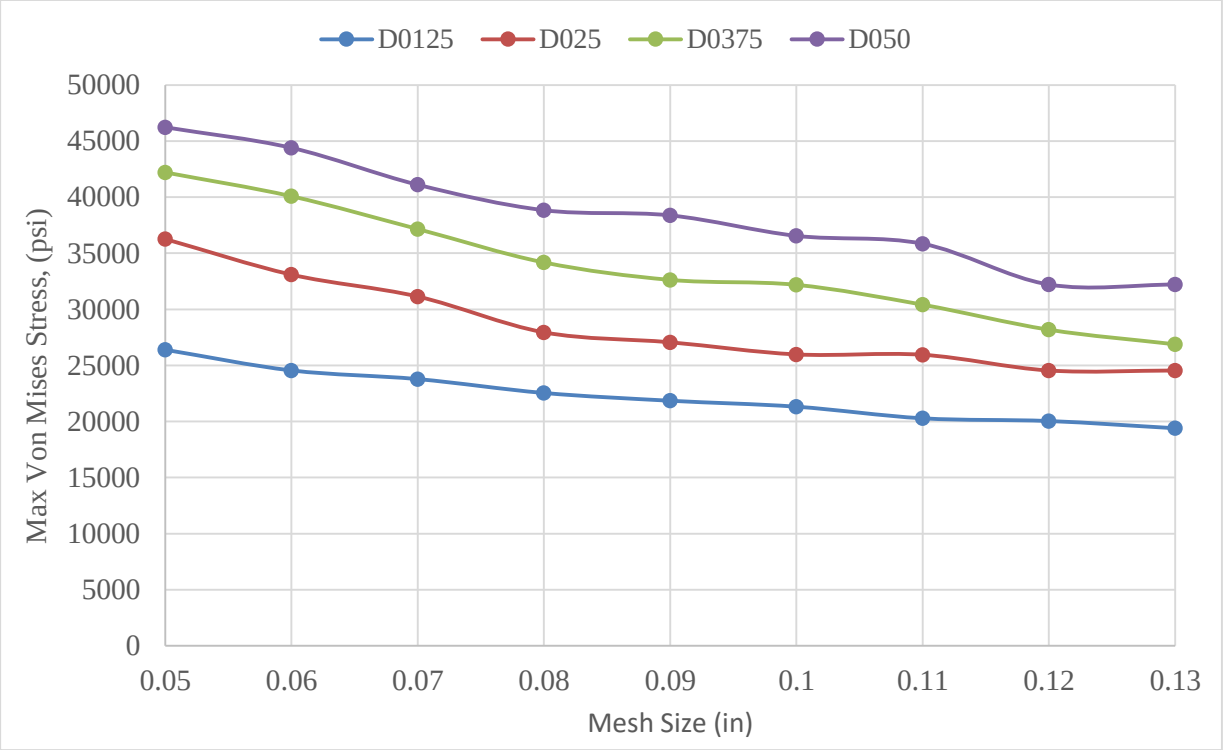

Figure 3.12. Maximum Von Misses Stress of bottom ply for different notch diameter.

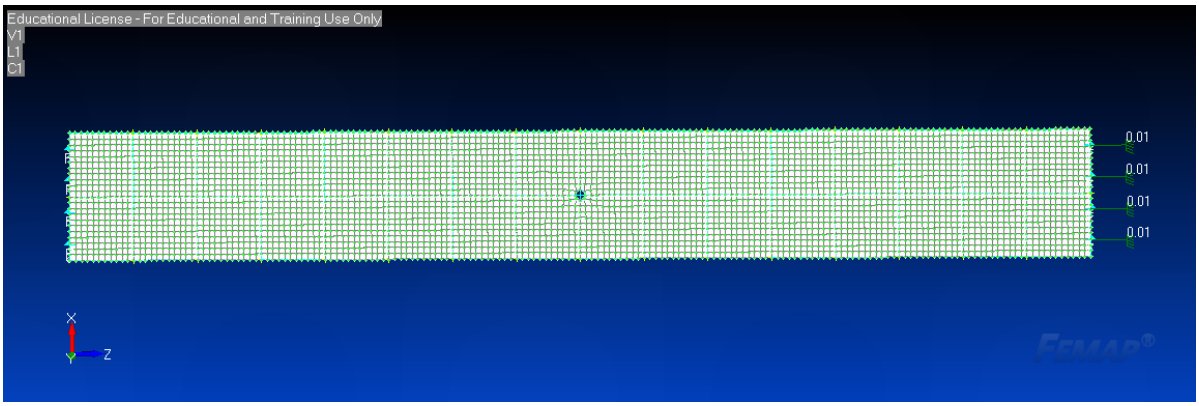

Figure 3.13. Mesh of notched specimen with a notch diameter of 3.18 mm (0.125 in)

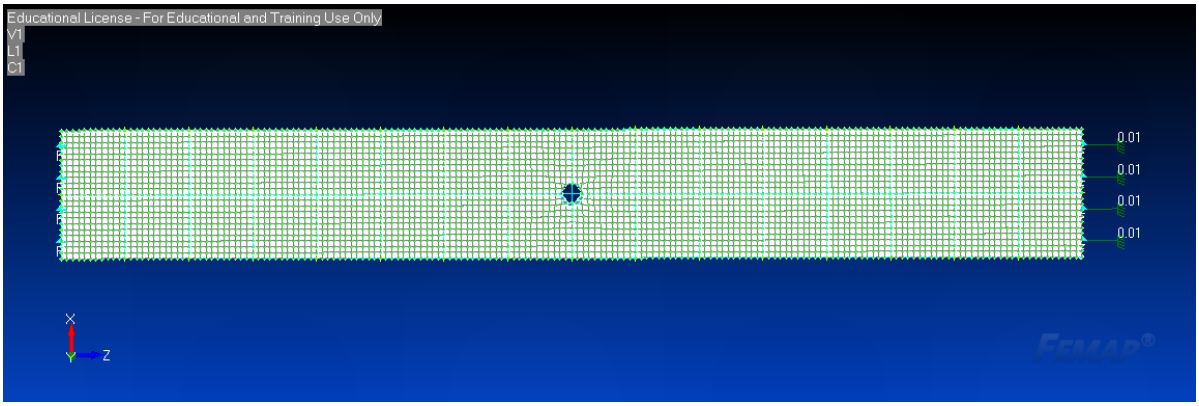

Figure 3.14. Mesh of notched specimen with a notch diameter of 6.35 mm (0.25 in)

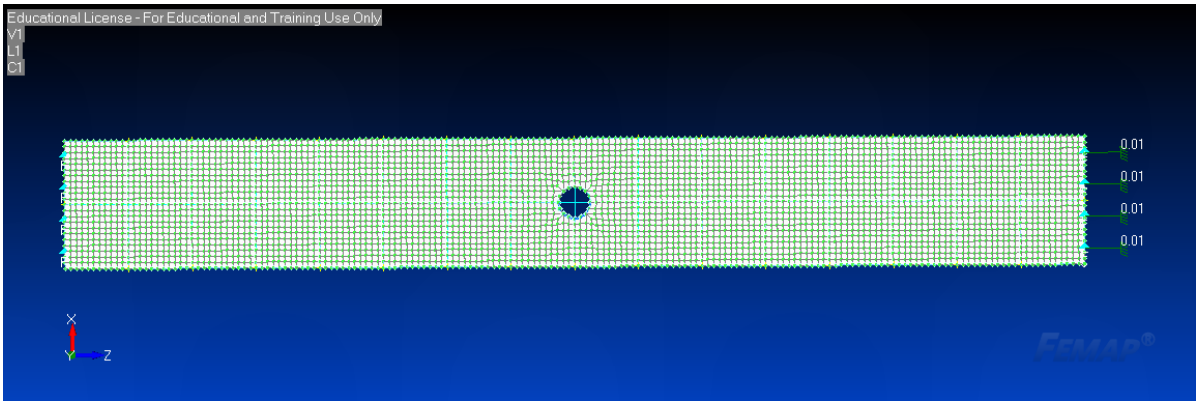

Figure 3.15. Mesh of notched specimen with a notch diameter of 9.53mm (0.375 in).

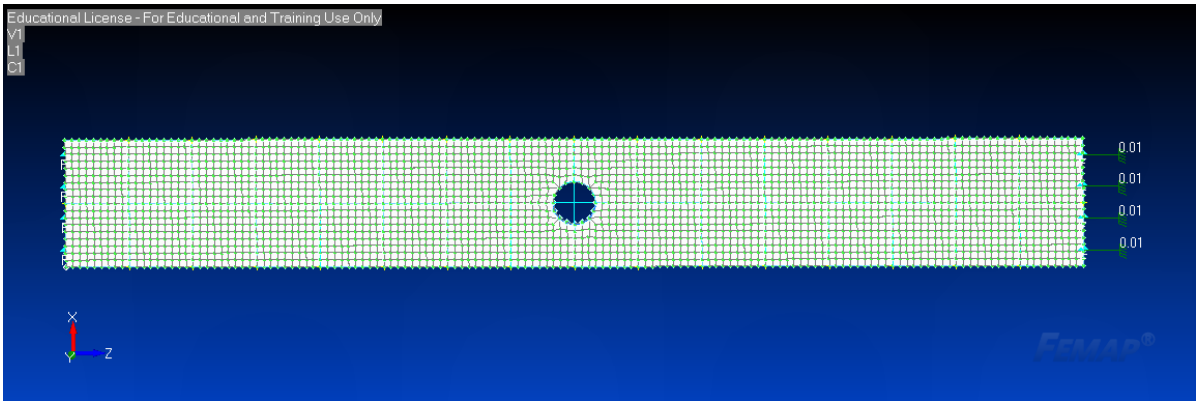

Figure 3.16. Mesh of notched specimen with a notch diameter of 12.7 mm (0.50 in)

3.3.4 *Quasi – Isotropic Material Properties*

HexMC is produced using chips of AS4/8552R unidirectional graphite epoxy pre-preg. Since the chips are randomly oriented, the elastic modulus of HexMC is expected to be equivalent, on average to the modulus of quasi-isotropic AS4/8552R continuous fiber based laminates. However, the unidirectional properties of AS/8552R have not been reported in the open literature. Hence, the elastic properties of AS4/8552R were predicted by using the closely related material system, AS4/8552 which were available [14, 15]. Table 3.5 reports the available properties of unidirectional AS4/8552 [14]. Classical lamination theory (CLT) was used to predict the quasi-isotropic stiffness of AS4/8552R using the AS4/8552 properties and were compared to the quasi-isotropic stiffness for HexMC. Table 3.6 summarizes properties reported for HexMC [15]. Both the quasi-isotropic stiffness obtained from CLT were substantially different reporting values that were about 18% higher than the average modulus reported for HexMC. To achieve quasi-isotropic stiffness that match the elastic properties reported for HexMC, the predicted quasi-isotropic stiffness were adjusted downward. Table 3. 7 summarizes the material properties used in this study.

Table 3.5. Properties for AS4/8552 Graphite-Epoxy Prepreg at Room Temperature

	E_{11}	E_{22}	υ_{12}	G_{12}
AS4/8552 properties [14]	141.32 GPa (20.5 Msi)	10.0 GPa (1.45 Msi)	0.32	5.28 GPa (0.766 Msi)

Table 3.6. Properties of HexMC at Room Temperature

	E_{11}	E_{22}	υ_{12}	G_{12}
HexMC properties [15]	131.69 GPa (19.1 Msi)	9.24 GPa (1.34 Msi)	0.302	4.83 GPa (0.70 Msi)

Table 3.7. Material Properties used in this study

	E_{11}	E_{22}	υ_{12}	G_{12}
Properties used in this study	118 GPa (17.1 Msi)	8.00 GPa (1.16 Msi)	0.32	4.45GPa (0.646 Msi)

Chapter 4. STIFFNESS PREDICTIONS BASED ON SLA

The stiffness predictions on the un-notched specimens with dimensions 38.1 mm (1.5 in) and 305 mm (12 in) were done based on the stochastic laminate analogy. Five tensile specimens with thicknesses of 1.02 mm (0.04 in), 2.03 mm (0.08 in), 2.30 mm (0.09 in), 3.05 mm (0.12 in) and 4.06 mm (0.16 in) were modeled. A total of 150 analyses were completed for each specimen thickness and the effective stiffness were obtained. Each specimen thickness represented the number of through-thickness chips. For example, the 1.02 mm (0.04 in) thick specimen represented 8 through-thickness chips, the 2.03 mm (0.08 in) represented 16 through-thickness chips, the 3.05 mm (0.12 in) thick specimen represented 24 through-thickness chips and finally the thickest specimen with thickness of 4.06 mm (0.16 in) represented 32 through-thickness chips. Based on the stochastic laminate analogy approach, the stiffness were obtained from the nominal stresses and nominal strains. Figure 4.1 shows a typical model with a contour plot of the resulting forces after a unit displacement of 0.254 mm (0.01 in) is applied to one end of the specimen. The nodal reaction forces at one fixed end is then summed and divided by the cross-sectional area to obtain the nominal stresses shown by equation 4.1.

$$\sigma_{axial} = \frac{R}{A} \tag{4.1}$$

The nominal strains on the other hand, were obtained by taking the enforced uniform unit displacement and dividing it by the specimen length, 305 mm (12 in).

$$\varepsilon_{axial} = \frac{\Delta l}{l} \tag{4.2}$$

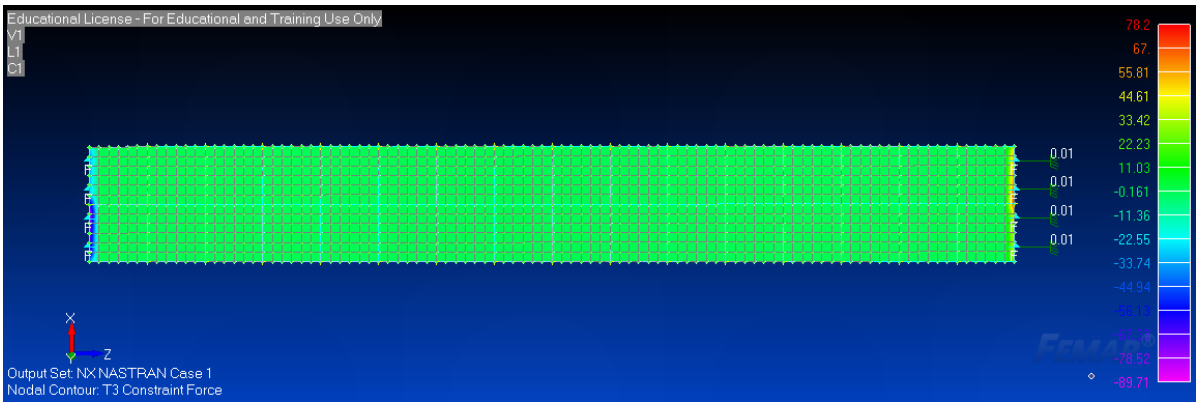

Figure 4.1. Resulting axial forces of a typical un-notched model.

4.1 B-MAX AND B-BASIS DEFINITIONS

Composites tend to have more variability than metals due to several factors which include fiber and resin materials, pre-preg manufacturing, material handling, stacking sequence, environmental conditions and testing techniques. Advanced statistical methods which accounts for this variabilities are needed to establish material properties. Design allowable are statistically significant material properties which are compared to an applied value in margin of safety calculations. The A- and B-Basis are allowable that is an indication of the assurance that the minimum property will be exceeded. The focus on this study will be on the B-basis allowable since it is used in multiple load path design. The B-basis modulus is defined as the modulus in which 90% of the measured values exceed, associated with a 95% confidence level. The B-basis strength is defined in the same way as the B-basis modulus in the CMH 17 Handbook [16]. The B-Max modulus on the other hand, a definition developed at the UW [9] is the modulus value under which 90% of the modulus values fall 95% of the time.

4.2 B-MAX AND B-BASIS CALCULATIONS

The design allowable generation for the B-basis values were done following the guidelines presented in DOT/FAA/AR-03/19 “Material Qualification and Equivalency for Polymer Matrix Composite Material Systems: Updated Procedure” [17]. Statistical data obtained from the modulus data were the sample mean, sample standard deviation, coefficient of variance and the B-basis tolerance factor. The coefficient of variance is the measure of dispersion or scatter in a data set, and composite materials generally have a coefficient of variance that range from 4% to 10% [17]. The statistical analyses and design-allowable generation for the B-basis values are performed using a data reduction method that groups the data from all environments and batches to obtain statistical information. Several underlying assumptions were made to generate a valid design allowable. If the normality assumption is valid and accepted for the obtained data, the procedure outlined in [17] is used. If the normality assumption is not valid, the Weibull distribution as outlined in methodology presented by Shyprykevich [18] should be used.

The general procedure to compute the B-basis allowable begins with normalizing raw test data by volume fraction, collecting data grouping by test environment, calculating the sample mean and standard deviation for each environment, check to see if there are any outliers present, check the normality assumption in environmental groupings and compute the coefficient of variance. If the coefficient of variance is greater than 4%, the procedure continues on to normalizing each environment grouping by the sample mean and computing the B-basis tolerance factor and finally, the B-basis value. However, if the coefficient of variance is less than 4%, the data should be transformed by modifying the coefficient of variance. From this, the two important factors when considering the use of this methodology is, the validity of the normality assumption and the range of coefficient of variance.

Five tensile un-notched specimens with dimensions summarized in Table 2 of Section 3.1.1, were modeled and stochastic laminate analogy, outlined in Section 3 was performed. A total of 150 randomly-generated random layup volume elements were generated for each specimen thickness. The stiffness values were obtained for the 150 randomly-generated RLVEs and the B-basis were computed. Modifications were made to the methodology presented in [17] to eliminate the steps which include normalizing data from different batches and environments. Since the data were obtained from finite element analysis, similar environmental conditions were enforced. The modified steps done to compute the B-basis values were presented accordingly in the next section.

4.2.1 *Sample Mean and Standard Deviation*

The initial steps of the modified design generation allowable procedure was obtaining the sample mean and standard deviation of a total of 150 analysis. Table 4.1 summarizes the mean and standard deviation for all 150 analysis for the five specimen thickness. The sample mean, $\bar{x}$ and standard deviation, s^2 for the data set was computed using the equations 4.3-4.4 [19].

$$\bar{x} = \frac{1}{n}\sum_{i=1}^{n} x_i \tag{4.3}$$

$$s = \frac{1}{(n-1)^{\frac{1}{2}}}\sum_{i=1}^{n}(x_i - \bar{x})^{\frac{1}{2}} \tag{4.4}$$

Where:

$\bar{x}$ = sample mean

x_i = stiffness values

n = total number of data points

s^2 = sample standard deviation

Table 4.1. Sample mean and standard deviation

Specimen Thickness	Sample Mean	Standard Deviation
1.02 mm (0.04 in)	39.44 GPa (5.72 Msi)	2.83 GPa (0.410 Msi)
2.03 mm (0.08 in)	45.51 GPa (6.60 Msi)	2.28 GPa (0.331 Msi)
2.30 mm (0.09 in)	45.71 GPa (6.63Msi)	1.80 GPa (0.259 Msi)
3.05 mm (0.120 in)	47.02 GPa (6.82 Msi)	1.63 GPa (0.237 Msi)
4.06 mm (0.160 in)	47.92 GPa (6.95 Msi)	1.40 GPa (0.203 Msi)
5.80 mm (0.23 in)	48.67 GPa (7.06 Msi)	1.17 GPa (0.169 Msi)
9.40 mm (0.37 in)	49.53 GPa (7.18 Msi)	0.97 GPa (0.14 Msi)

4.2.2 *Outliers*

The next step of the modified design-allowable generation procedure was to check if there are outliers present in this study. Outliers can have a substantial influence on the statistical analysis. Typically, methods used to check for outliers are, a visual representation of graphical plots of the data or a quantitative procedure. The quantitative procedure constitutes the Maximum Normal Residual (MNR) method, as suggested by MIL-HDBK-17 [16]. Since this study is entirely numerical, there are no outliers present.

4.2.3 *Normal Distribution*

The most widely used model for the distribution of a random variable is a normal distribution, also referred to as a Gaussian distribution. In this study, the normality check is done by visually representing graphical plots of the data distribution with a best-fit normal curve. Engineering judgement was used to check for the validity of the normal distribution. The data was sorted in an ascending order and the probability of survival at each value was computed using equation 3 [17].

$$Probability\ of\ survival\ at\ x_i = 1 - \frac{\mathrm{i}}{\mathrm{n+1}} \tag{4.5}$$

Where:

n = total number of data points

i = rank of stiffness values, x_i in sorted list

x_i = stiffness values at rank i in sorted list

The data was then normalized by dividing the individual stiffness by the mean stiffness for all the data points. Normalizing will results in the overall data having a mean of 1.0. Figure 20 shows the normal distribution of the stiffness values obtained from numerical analysis against the

normalized values for a specimen of thickness 2.03 mm (0.08 in). Visual inspection of the best normal fit, shows the assumption of normality is valid.

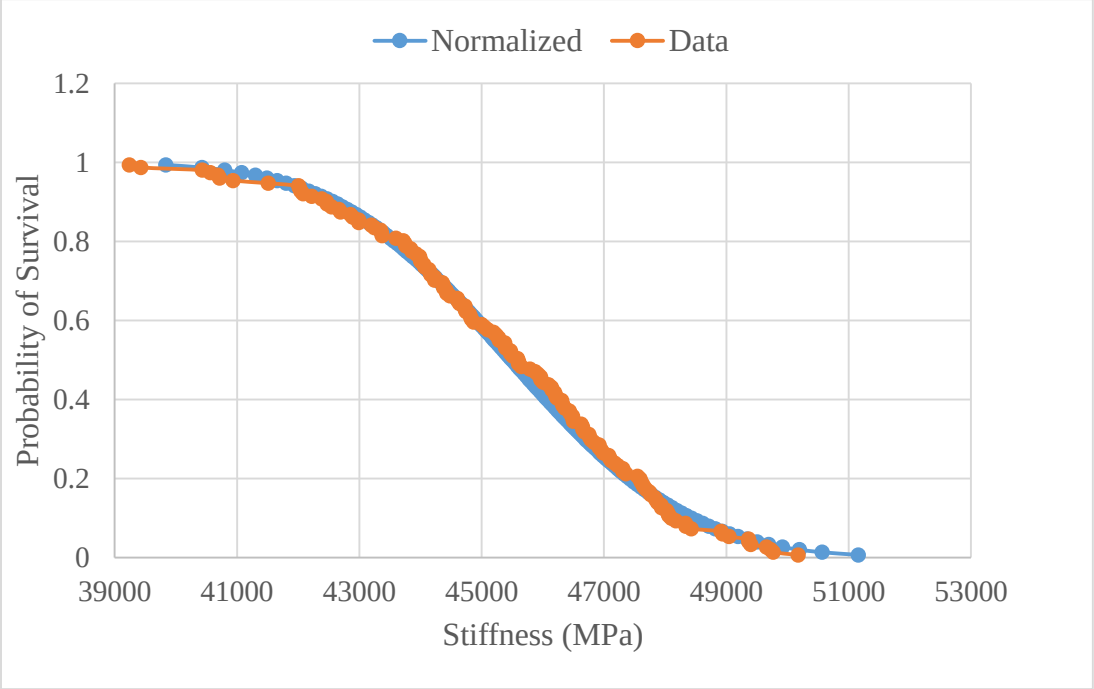

Figure 4.2. Normal probability functions of stiffness data

4.2.4 *Coefficient of Variance*

Next, the coefficient of variance was computed to account for the variability or scatter in the data. If the value of coefficient of variance, s^2 is small, then there is relatively little variability in the data. Conversely, if the coefficient of variance is large, the variability is relatively large. Typical composite materials have a coefficient of variance in the range of 4% to 10%. Table 4.2. summarizes the coefficient of variance obtained through equation 4.6 [19].

$$s^2 = \frac{1}{n-1}\sum_{i=1}^{n}(x_i - \bar{x})^2 \tag{4.6}$$

Where:

$\bar{x}$ = sample mean of the stiffness values

x_i = stiffness values

n = total number of data points

s^2 = sample coefficient of variance

Table 4.2. Coefficient of Variance

Specimen Thickness	Coefficient of Variance
1.02 mm (0.04 in)	7.18 %
2.03 mm (0.08 in)	5.02 %
2.30 mm (0.09 in)	3.91 %
3.05 mm (0.120 in)	3.48 %
4.06 mm (0.160 in)	3.00 %
5.80 mm (0.23 in)	2.40 %
9.40 mm (0.37 in)	2.00 %

Coefficient of variances of the numerical stiffness values fall in the range of 2% to 10%. Lower coefficients of variation could be due to the specimen fabrication, testing by a single laboratory while higher coefficients of variation indicates the lack of material and processing control. From Table 9, the coefficient of variance fall within or close to the range from 2% to 10%. The two lowest specimen thickness, 1.02 mm (0.04 in) and 2.03 mm (0.08 in) have coefficient of variance that fall in the higher range which indicates a higher dispersion of sample data. Ideally, lower coefficient of variances resemble better material and processing control, however since these

analysis were purely numerical and based on a random stacking sequence the measure of coefficient of variance is not a good benchmark of predicting the accuracy or dispersion of this data.

4.2.5 *B-Basis and B-Max Tolerance Factor*

The tolerance factor is estimated by the number of standard deviations, kb which can be approximated by equation 4.7 [17]. The tolerance factor for the normal distribution is based upon the total number of samples.

$$k_B = z_B\sqrt{\frac{f}{Q}} + \sqrt{\frac{1}{n*C_B} + \left(\frac{b_B}{2C_B}\right)^2} - \frac{b_B}{2C_B} \tag{4.7}$$

Where:

n = total number of stiffness samples

z_B = standard normal variable.

b_B, c_B = coefficients

Q = coefficient dependent on the variance degrees of freedom

f = degrees of freedom for the variance

Since the B-basis stiffness is defined as a value in which 90% of the measured values exceed with a 95% confidence level, while the B-max stiffness is the value that exceeds 90% of the measured values with a 95% confidence level, the standard normal random variable, z_B was taken as 1.28115 (90% probability) [17]. The coefficients b_B and c_B are expressed in equations 4.8 and 4.9 [17].

$$b_B(f) = 1.1372\frac{1}{\sqrt{f}} - 0.49162\frac{1}{f} + 0.18612\ \frac{1}{f\sqrt{f}} \tag{4.8}$$

$$c_B(f) = 0.36961 + 0.0040342\frac{1}{\sqrt{f}} - 0.71750\frac{1}{f} + 0.19693\ \frac{1}{f\sqrt{f}} \qquad (4.9)$$

Where:

b_B, c_B = coefficients of interest

f = degrees of freedom for the variance

The degrees of freedom for the variance, f is denoted by the total number of data points subtract 2, $\mathrm{n} - 2$. Since the degrees of freedom, f exceeds a value of 3 in this study ($f = n - 2 = 148$) , the value of Q can be approximated by equation 4.10 [17].

$$\mathrm{Q} = \mathrm{f} - 2.327\sqrt{\mathrm{f}} + \ 1.138 + \ 0.6057\frac{1}{\sqrt{\mathrm{f}}} - 0.3287\frac{1}{f} \qquad (4.10)$$

4.2.6 *B-Basis and B-Max Values*

The final step is of this design-allowable generation procedure was to calculate the B-basis and B-max values. The aerospace industry has defined the B-basis allowable [16] which can be calculated using equation 4.11 [17].

$$B_{basis} = \ \bar{\mathrm{x}} - (\mathrm{k_B})\mathrm{s} \qquad (4.11)$$

Where:

B = B-basis stiffness

k_B = tolerance factor

s = standard deviation of stiffness data

From the knowledge of engineering statistics, the B-basis allowable is equivalent to the lower confidence of a sample data with 95% confidence interval where the lower confidence is obtained by subtracting the product of the standard normal variable ($z_{\alpha/2}$) with the sample standard deviation (σ) normalized by the sample size (n) from the sample mean ($\bar{x}$). Equation 4.12 illustrates the lower confidence computation in engineering statics [19].

$$\text{lower confidence} = \bar{x} - (z_{\alpha_{/2}}\sigma)/\sqrt{n} \tag{4.12}$$

$$\text{upper confidence} = \bar{x} + (z_{\alpha_{/2}}\sigma)/\sqrt{n} \tag{4.13}$$

Where:

σ = standard deviation of sample data

$\bar{x}$ = sample mean

$z_{\alpha/2}$ = standard normal variable

The upper confidence shown in equation 4.13 [19], is defined in a similar manner to the lower confidence, instead of subtracting the normalized standard deviation from the sample mean, the normalized standard deviation is added to the sample mean. The procedure outlined in [17] includes the computations of the standard normal variable, the degrees of freedom and the coefficients that are dependent on the degrees of freedom to account for variability in material properties in composites. The engineering statistical computation of the lower and upper tolerance, on the other hand is a generic formula that does not account for significant variability in the sample data.

By inspection, the B-basis design allowable equation obtained from [17], matches the lower confidence definition, where the product of the tolerance factor and the standard deviation is essentially the normalized standard deviation. The B-basis equation, as given in equation 9 does affirm the definition of B-basis, which is the value in which 90% of the measured values exceed

95% of the time. Conversely, the B-max can be obtained by computing the value in which 90% of the measured values fall under, 95% of the time which means the upper confidence engineering statistic definitions could be manipulated to obtain the B-max stiffness value. By adding the product of the tolerance factor and the sample standard deviation to the sample mean of the stiffness data, the resulting value does indeed exceed 90% of the measured value. Hence, the B-max equation is given in equation 4.14.

$$B_{max} = \bar{x} + (k_B)s \tag{4.14}$$

Where:

B = B-basis stiffness

k_B = tolerance factor

s = standard deviation of stiffness data

A way to check if the computation for the B-basis and B-max values are valid, is to plot the B-basis, B-max and average stiffness values. By visual inspection, the average values should fall in between the B-max and B-basis values since the latter two enfolds the sample data with 90% probability.

4.3 B-MAX AND B-BASIS RESULTS

The calculated B-basis and B-max stiffness values were compared with the average modulus values and tabulated in Table 4.3. Figure 4.3 shows the distribution of the B-basis, average and B-max stiffness values for the five specimens with different thickness tested. The B-basis and average values show an increasing trend as the specimen thickness increases. The B-max values on the other hand, follows the same increasing trend up to the specimen with thickness of 2.30 mm

(0.09 in), then it decreases and increases again. The results shows that as the number of plies in a specimen increases, the stiffer the specimen gets.

Table 4.3. B-basis, Average and B-max stiffness

Specimen Thickness	B-basis Stiffness	Average Stiffness	B-max Stiffness
1.02 mm (0.04 in)	35.37 GPa (5.13 Msi)	39.44 GPa (5.72 Msi)	43.44 GPa (6.30 Msi)
2.03 mm (0.08 in)	42.26 GPa (6.13 Msi)	45.51 GPa (6.60 Msi)	48.75 GPa (7.07 Msi)
2.30 mm (0.09 in)	43.16 GPa (6.26 Msi)	45.71 GPa (6.63Msi)	48.26 GPa (7.00 Msi)
3.05 mm (0.120 in)	44.68 GPa (6.48 Msi)	47.02 GPa (6.82 Msi)	49.37 GPa (7.16 Msi)
4.06 mm (0.160 in)	45.92 GPa (6.66 Msi)	47.92 GPa (6.95 Msi)	49.92 GPa (7.24 Msi)
5.80 mm (0.23 in)	47.00 GPa (6.82 Msi)	48.67 GPa (7.10 Msi)	50.34 GPa (7.30 Msi)
09.4 mm (0.37 in)	48.15 GPa (6.98 Msi)	49.53 GPa (7.18 Msi)	50.91 GPa (7.38 Msi)

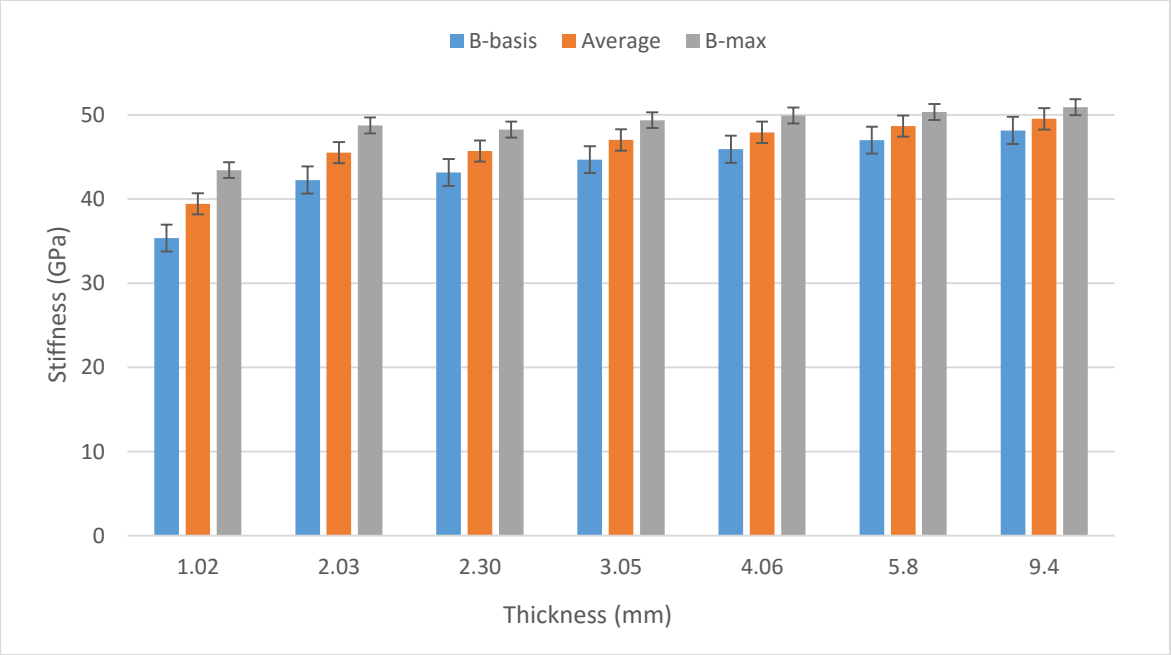

Figure 4.3. B-max, average and B-basis stiffness values for un-notched specimens

The stiffness predictions for the 7 specimen thickness were compared to proprietary Hexcel data and shown in Figure 4.4. The trends of the average and B-basis UW values agree qualitatively with proprietary Hexcel data.

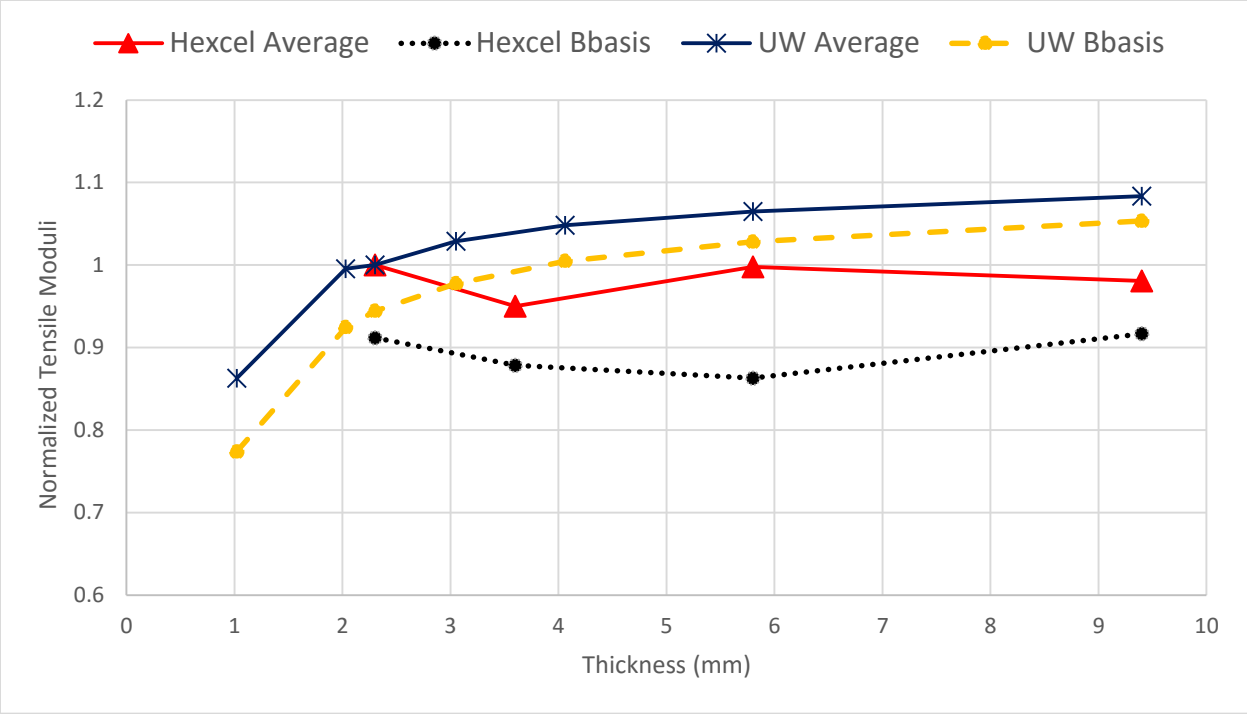

Figure 4.4. Comparison between measured and predicted tensile moduli. Hexcel measurements are normalized to average measured value for 2.3 mm thick specimens, while UW predictions are normalized to average predicted value for 2.3 mm thick specimens

Chapter 5. STRENGTH PREDICTIONS BASED ON SLA

5.1 MODELING

Strength predictions of HexMC notched and un-notched specimens were done based on a damage accumulation model applied to each finite element. The damage accumulation model used in this study is the ply discount method. A ply discount method is an approach which utilizes a fracture criterion to determine a critical or a region most susceptible to failure in a specimen. Initially, a finite element modeling approach is performed, as mentioned in Section 3.31 where the material properties are defined, model is discretized into RLVEs and finite elements, and boundary/loading conditions are applied. A random stacking sequence is then defined for each RLVE and is unique from its neighboring RLVEs. A finite element analysis is then performed, the resulting stresses are extracted to compute a new load that will cause more chip failure. A new load is then applied, and the properties of the failed chip are reduced and this process was repeated until the final fracture criterion is met. Figure 5.1 shows a flow chart that illustrates the ply discount procedure. The final fracture criteria is discussed in Section 5.1.2. The ply discount scheme was done based on the stochastic laminate analogy with the application of finite element modeling.

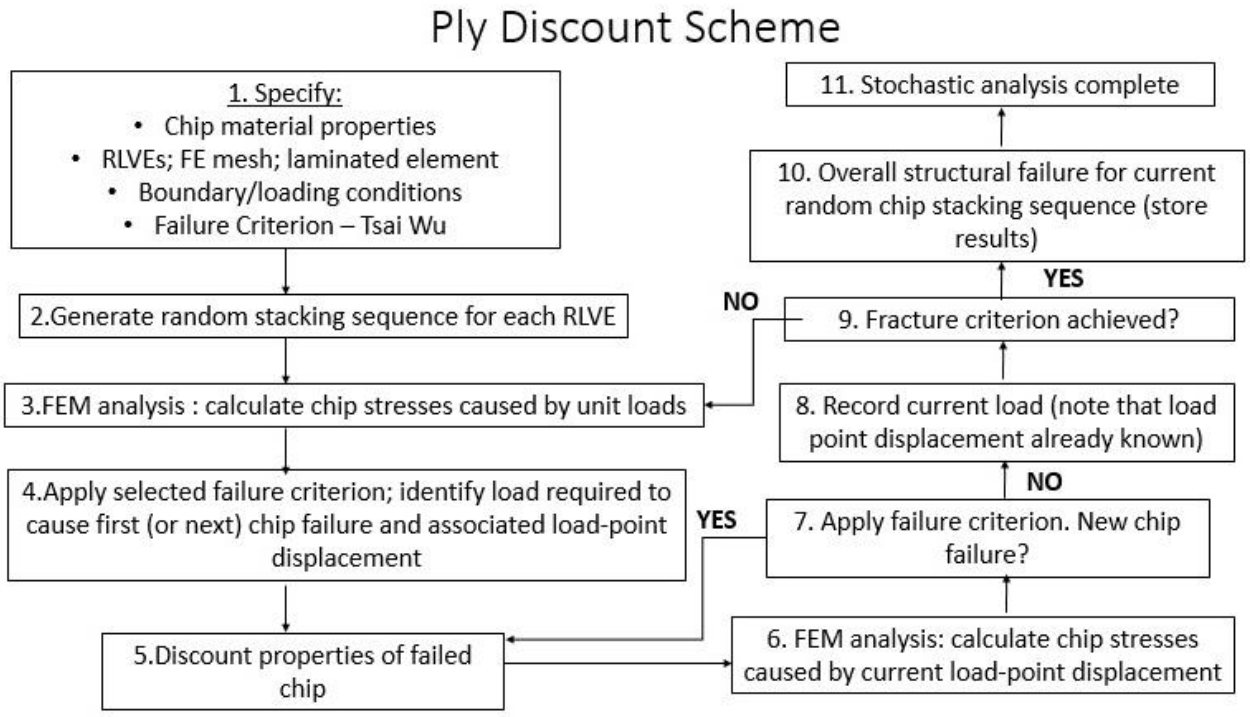

Figure 5.1. Flow Chart of the Ply Discount Scheme.

5.1.1 *Material Properties*

The ply discount process illustrated in the flow chart in Figure 5.1 requires two sets of material properties. The first set of material properties used in the preliminary ply discount procedure was listed in Table 3.7. When chip failure occurred from the first set of material properties, the properties of the failed chip was then reduced to prevent the same chip from failing. The material properties for composites are divided into fiber dominated properties, the elastic stiffness in the fiber direction, E_{11} and matrix dominated properties, elastic stiffness in the matrix direction, E_{22} and the shear modulus, G_{12}. For the second set of properties, the fiber dominated properties was arbitrarily reduced by 90% and the matrix dominated properties were reduced by 30%. Table 5.1 summarizes the material properties used in preliminary ply discount procedure, and the weakened reduced properties applied to the failed chips.

Table 5.1. Material Properties used in the ply discount scheme

	E_{11}	E_{22}	υ_{12}	G_{12}
Initial set of properties	118 GPa (17.1 Msi)	8.00 GPa (1.16 Msi)	0.32	4.45GPa (0.646 Msi)
Weakened Properties	106 GPa (15.39 Msi)	2.40 GPa (0.348 Msi)	0.32	1.34 GPa (0.194 Msi)

5.1.2 *Final Structural Failure*

A final fracture criteria that is conservative is essential in determining the region of the specimen most susceptible to failure. There are several final fracture criteria that was defined and experimented with in this study. The final fracture conditions defined in order are:

- Final fracture happened when all chips within a single element have failed
- Final fracture happened when a specified number of chips have failed

The overall computation time was the least for the first fracture definition, that is when all chips within a single element have failed and longest for the last definition of fracture. With the first definition of fracture criterion, a single analysis took about 18 – 95 hours to complete, with the last final fracture definition however, a single analysis took up to 92 hours to complete. Hence, most of the stochastic laminate analogy conducted in this study was done using the final fracture criteria at which when all chips in a single element have failed, to account for reasonable computation times. Figure 5.2 shows a typical flow chart of the stochastic laminate analogy done when the first final fracture definition was implemented.

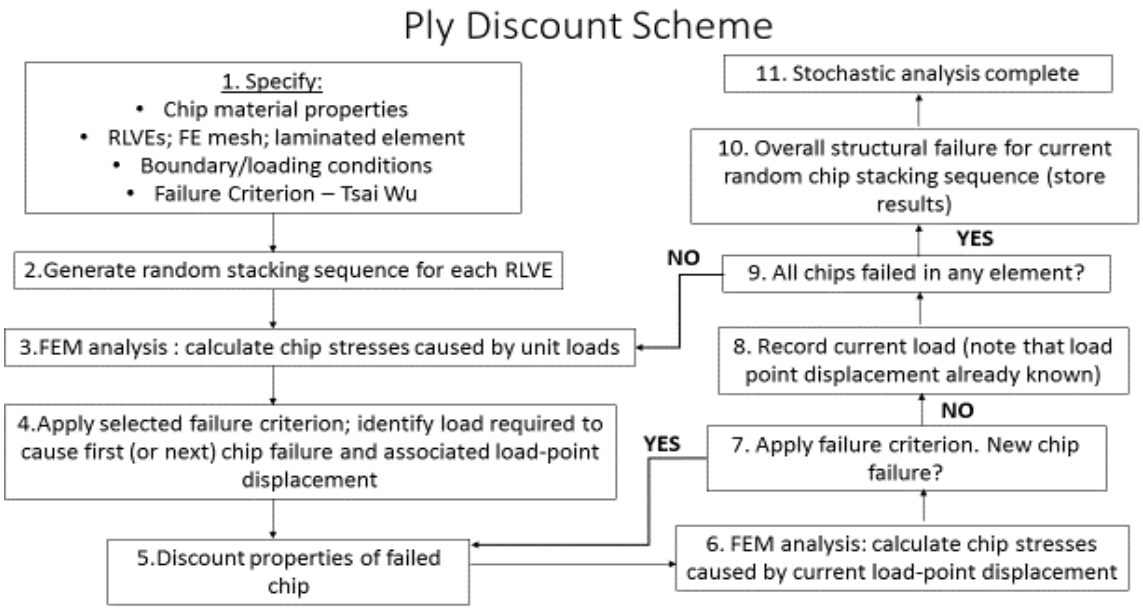

Figure 5.2.. Flow chart of the Ply Discount Scheme implementing the first final fracture condition.

5.2 TSAI – WU FAILURE CRITERIA

A failure criteria is needed in structural analysis to account for coupling between the stresses in the fiber direction and the matrix direction. The Tsai-Wu criteria was chosen in this study because it collapses close to the Von Mises criteria, and it accounts for coupling between individual fiber and matrix stress components. Through the Tsai-Wu constants, the differences in tensile and compressive strengths are also accounted for, using the Tsai-Wu criteria [20]. Since this finite element modeling was done in FEMAP NX Nastran, it was important to use a failure criteria that is built in FEMAP Nastran and the Tsai-Wu failure criteria was one of them. The Tsai-Wu criterion predicts that if the inequality in equation 5.1 is satisfied for a 3-D state of stress, failure will not occur [20]. A plane stress state was assumed in this study since the specimens used in this study were relatively thin, resulting in very small out-of-plane stresses. The following two sub-sections explains in details the failure strengths and the Tsai-Wu constants used in this study.

$$X_1\sigma_{11} + X_2\sigma_{22} + X_3\sigma_{33} + X_{11}\sigma_{11}^2 + X_{22}\sigma_{22}^2 + X_{33}\sigma_{33}^2 + X_{44}\tau_{23}^2 + X_{55}\tau_{13}^2 + X_{66}\tau_{12}^2 + 2X_{12}\sigma_{11}\sigma_{22} + 2X_{13}\sigma_{11}\sigma_{33} + 2X_{23}\sigma_{22}\sigma_{33} < 1 \quad (5.1)$$

Where:

$X_1, X_2, X_3, X_{11}, X_{22}$ = Tsai-Wu coefficients of normal stresses

$X_{33}, X_{44}, X_{55}, X_{66}$ = Tsai-Wu coefficients of the square of normal stresses

X_{12}, X_{13}, X_{23} = Tsai-Wu coefficients of the product of normal stresses

$\sigma_{11}, \sigma_{22}, \sigma_{33}$ = Normal stress resulting from the unit load applied

$\tau_{12}, \tau_{23}, \tau_{13}$ = Shear stress resulting from the unit load applied

5.2.1 *HexMC Failure Strengths*

The failure strengths used in this study were reduced from the failure strength properties of the unidirectional AS4/8552 graphite-epoxy prepreg. Table 5.2 lists the failure strength values of AS4/8552 unidirectional pre-preg at room temperature [14]. The tensile and compressive strengths in the fiber directions were given, however only the tensile strength in the matrix direction were provided. The compressive strength in the matrix direction were assumed to be equal to the tensile strength in the matrix direction. The values in Table 12 were used as reference values, in which the tensile strengths in the matrix and fiber directions and the in-plane shear strength were reduced by~54%. The compressive strengths in the fiber direction were reduced by~38%. The resulting compressive strength in the matrix direction were obtained by multiplying the ratio of transverse compressive strength to the transverse tensile strength with the reduced tensile strength in the matrix direction summarized in equation 5.2. Table 5.3 summarizes the reduced failure strength values used in this study. As described in the ply discount scheme flow chart in Figure 14, when a chip fails, the elastic material properties of that

failed chip are discounted while the failure strengths of the failed chip are increased by a magnitude of 10 to prevent the same chip from failing. Table 5.4 summarizes the new failure strengths applied to a failed chip.

$$\sigma_{22}^{C} = \sigma_{22}^{T} \text{ x } \frac{Tc}{Tt} \tag{5.2}$$

Where:

σ_{22}^{C} = Compressive strength in the matrix direction, 90^o compressive strength

σ_{22}^{T} = Tensile strength in the matrix direction, 90^o tensile strength

Tc = Transverse compressive strength

Tt = Transverse tensile strength

Table 5.2. Failure Strengths of AS4/8552 Graphite-Epoxy uni-directional Prepreg

0^o Strength		90^o Strength		Transverse Strength		In-Plane Shear Strength
Tensile	Compressive	Tensile	Compressive	Tensile	Compressive	
2207 MPa (320 ksi)	1531 MPa (222 ksi)	81 MPa (11.7 ksi)	81 MPa (11.7 ksi)	64 MPa (9.27 ksi)	268 MPa (38.85 ksi)	114 MPa (16.6 ksi)

Table 5.3. Failure Strengths used in this study

0^o Strength		90^o Strength		In-Plane Shear Strength
Tensile	Compressive	Tensile	Compressive	
1014 MPa (147 ksi)	950 MPa (137.8 ksi)	37 MPa (5.38 ksi)	48 MPa (6.89 ksi)	53 MPa (7.626 ksi)

Table 5.4. New Failure Strengths used on failed chips

0^o Strength		90^o Strength		In-Plane Shear Strength
Tensile	Compressive	Tensile	Compressive	
10 GPa (1470 ksi)	9.5 GPa (1378 ksi)	3.7 GPa (53.8 ksi)	480 MPa (68.9 ksi)	530 MPa (76.26 ksi)

5.2.2 *Tsai – Wu Constants*

The tensile specimens modeled were subjected to a state of plane stress within the 1-2 plane, which reduces the Tsai-Wu criterion from equation 5.1 to equation 5.3 [21]. The plane stress condition results in six constants, five of which can be obtained directly from the failure strengths as illustrated in equations 5.4 to 5.9, while the other constant, X_{12} can be determined either by conducting a biaxial test or by equation 5.9 [20] . Since the tensile composite specimens modeled are relatively thin, conducting a biaxial tests is difficult, the constant X_{12} is calculated using equation 5.9. Table 5.5 summarizes the Tsai-Wu constants used in this study.

$$X_1\sigma_{11} + X_2\sigma_{22} + X_{11}\sigma_{11}^2 + X_{22}\sigma_{22}^2 + X_{66}\tau_{12}^2 + 2X_{12}\sigma_{11}\sigma_{22} < 1 \qquad (5.3)$$

Where:

X_1, X_2, X_{11}, X_{22} = Tsai-Wu coefficients of normal stresses

X_{12} = Tsai-Wu coefficients of the product of normal stresses

σ_{11}, σ_{22} = Normal stress resulting from the unit load applied

τ_{12} = Shear stress resulting from the unit load applied

$$X_1 = \frac{1}{\sigma_{11}^{fT}} - \frac{1}{\sigma_{11}^{fC}} \quad (5.4)$$

$$X_2 = \frac{1}{\sigma_{22}^{fT}} - \frac{1}{\sigma_{22}^{fC}} \quad (5.5)$$

$$X_{11} = \frac{1}{\sigma_{11}^{fT}\sigma_{11}^{fC}} \quad (5.6)$$

$$X_{22} = \frac{1}{\sigma_{22}^{fT}\sigma_{22}^{fC}} \quad (5.7)$$

$$X_{66} = \frac{1}{\sigma_{22}^{fT}\sigma_{22}^{fC}} \quad (5.8)$$

$$X_{12} = \frac{1}{\sqrt{X_{11}X_{22}}} \quad (5.9)$$

Table 5.5 Tsai-Wu constants used in this study

Tsai – Wu constants	X_1	X_{11}	X_2	X_{22}	X_{66}	X_{12}
	$-4.542e^{-7}$	$4.94e^{-11}$	$4.091e^{-5}$	$2.70e^{-8}$	$1.72e^{-8}$	$-5.77e^{-10}$

5.3 STRENGTH RESULTS

The strength predictions was performed based on a simple damage accumulation model, called the ply discount scheme described in Section 5.1. The ply discount scheme was applied to each finite element, with initial unit loads applied. Based on the ply discount scheme, the analysis was then completed following four structural fracture criteria explained in section 5.1.2. The results obtained from the ply discount scheme are presented in the following sections for the different structural fracture criteria. Computation times increased from the first structural fracture criteria in that order up to the fourth structural fracture criteria. As a result, most of the analysis performed were based on the first structural fracture criteria; when all plies in a single element failed.

5.3.1 *First Structural Failure Criteria of Un-notched*

The definition of the first structural fracture criteria defined in Section 5.1.2 is when all plies in a single element have failed. Strength predictions were done on un-notched and notched tensile specimens with dimensions summarized in Section 3.1.1 and 3.1.2. Since a single analysis took about 18-95 hours to complete, in efforts to reduce computation times, the strength predictions were done with un-notched specimens of length 178 mm (7 in) instead of 305 mm (12 in) as done for the stiffness predictions. Un-notched strength predictions were done only for the thickest specimen, 4.06 mm (0.16 in) and thinnest specimen, 1.02 mm (0.04 in), in contrast to the stiffness predictions. For each tensile notched and un-notched specimen thickness, five analysis were completed to predict the strengths. Table 5.6 summarizes the number of chip failure, failed element, computation time and maximum strength results for un-notched specimens with dimensions 38 mm (1.5 in) by 178 mm (7 in). The results show that the computation times for 32 ply thick specimen takes up to as long as 35 hours.

Table 5.6. Strength Results for two un-notched specimen thickness

Specimen Thickness	Analysis Number	Number of Chip Failure	Failed Element	Computation Time (hours)	Maximum Strength
1.02 mm (0.04 in)	1	699	474	2.38	91.66 MPa (13.30 ksi)
	2	787	131	2.61	108.77 MPa (15.78 ksi)
	3	773	109	2.59	152.87 MPa (22.17 ksi)
	4	494	150	1.70	109.59 MPa (15.90 ksi)
	5	435	193	1.51	133.64 MPa (19.38 ksi)
4.06 mm (0.16 in)	1	5336	433	17.14	221.73 MPa (32.16 ksi)
	2	9788	273	27.85	222.58 MPa (32.29 ksi)
	3	10363	658	30.99	268.11 MPa (38.89 ksi)
	4	6592	320	19.62	220.73 MPa (32.02 ksi)
	5	11796	80	34.94	246.76 MPa (35.79 ksi)

Figure 5.3 shows the scatter of chip failure for the un-notched specimen with thickness 1.02 mm (0.04 in) and figure 5.4 shows the scatter of chip failure for the specimen with thickness 4.06 mm (0.16 in). The chip failure is distributed randomly throughout the specimen due to the non-symmetric and random stacking sequence of the specimen, the heterogeneous nature of DFCs.

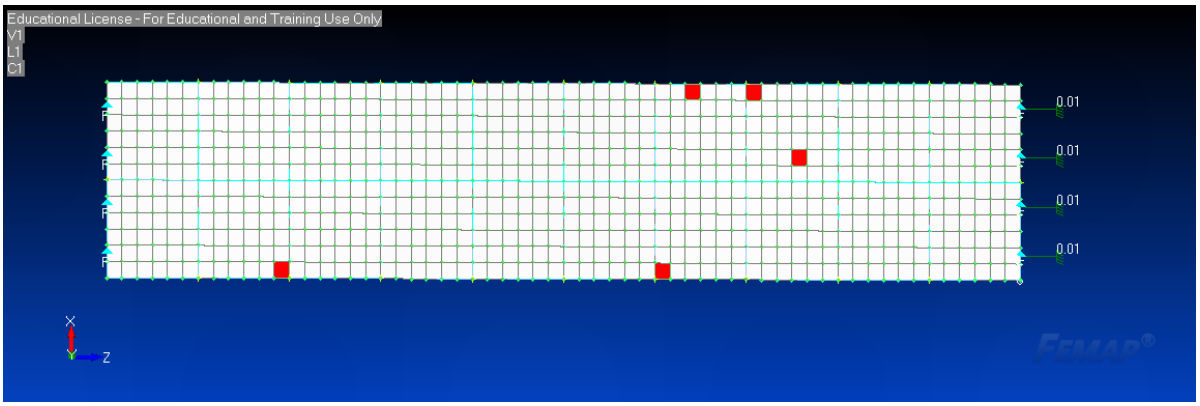

Figure 5.3. Chip failure distribution of un-notched specimen thickness 1.02 mm (0.04 in)

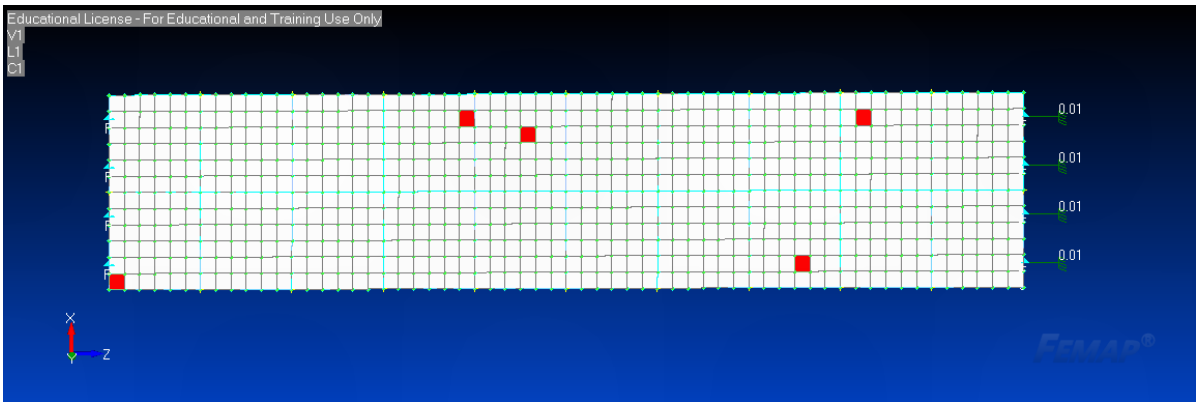

Figure 5.4. Chip failure distribution of un-notched specimen thickness 4.06 mm (0.16 in)

Figure 5.5 and Figure 5.6 shows a plot of the strength versus strain for both the un-notched specimen thickness of 1.02 mm (0.04 in) and 4.06 mm (0.16 in). The slope for the different analysis for each specimen thickness varies with differences ranging from 13.10% to 33.3%. The strengths for the thicker specimen are about double the magnitude of strengths of the thinner specimen because of the number of plies present in the specimen. Table 5.7 summarizes

the B-range and average maximum gross strength values. Figure 5.7 shows a bar chart of the calculated B-max, B-basis and average values for the two un-notched tensile specimens of thickness 1.02 mm (0.04 in) and 4.06 mm (0.16 in).

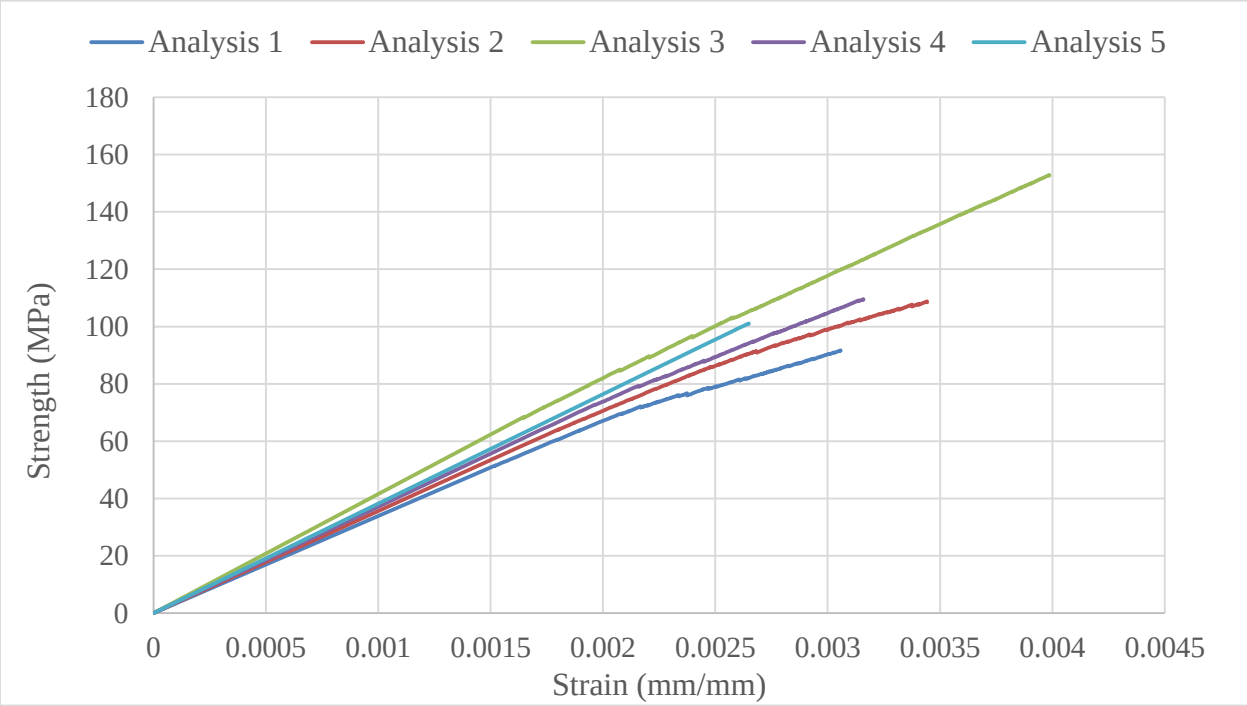

Figure 5.5. Strength versus strain curves for un-notched thickness of 1.02 mm (0.04 in).

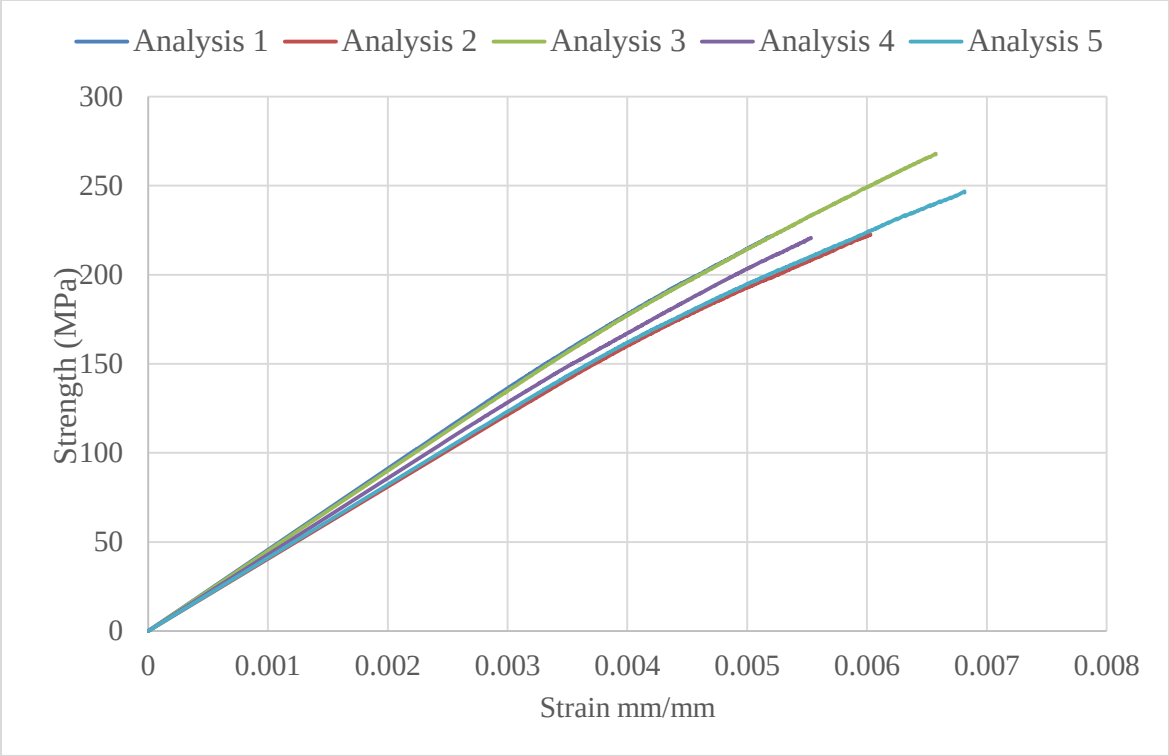

Figure 5.6. Strength versus strain curves for un-notched thickness of 4.06 mm (0.16 in).

Table 5.7. B-basis, Average and B-max Strength for un-notched specimens

Specimen Thickness	B-basis Strength	Average Strength	B-max Strength
1.02 mm (0.04 in)	20.85 MPa (3.02 ksi)	119.31 MPa (17.30 ksi)	217.76 MPa (31.6 ksi)
4.06 mm (0.16 in)	149.78 MPa (21.72 ksi)	235.98 MPa (34.23 ksi)	322.18 MPa (46.73 ksi)

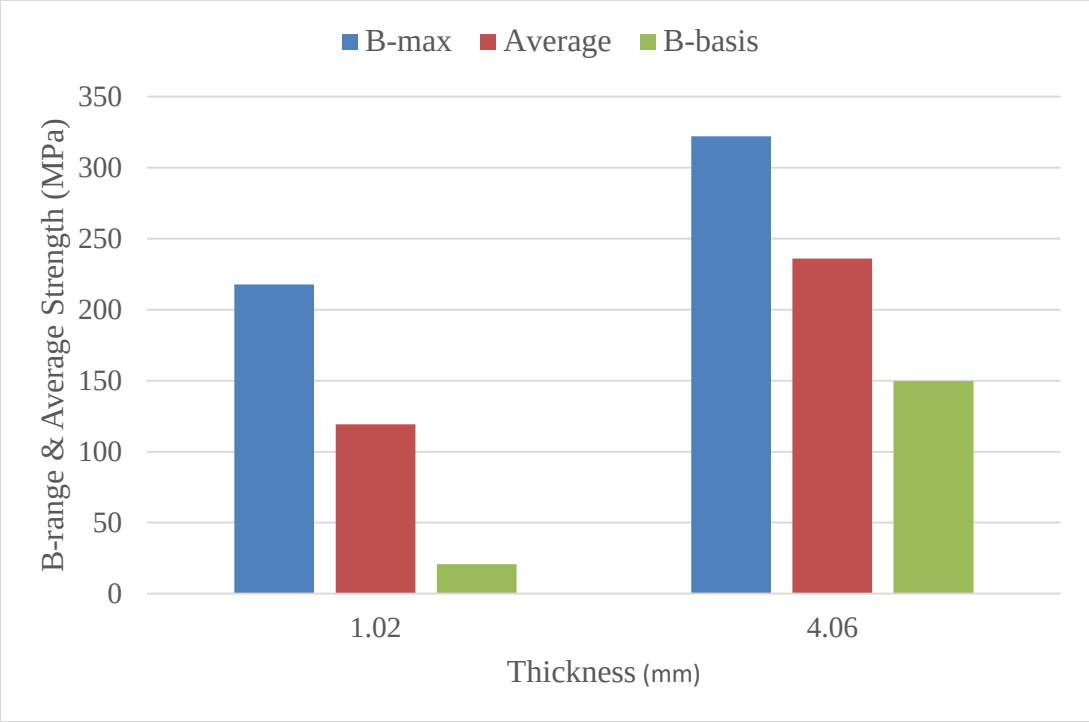

Figure 5.7. B-max, Average and B-basis strength values for un-notched specimens.

The B-max, B-basis and average strength values obtained from a total of five analysis is not a suitable range for strength values. This can be shown by a visual representation of the normalized maximum gross strength values against the predicted gross strength values. Figures 5.8 and 5.9 show a plot of the normalized strength values against the strength data. Both figures disobey the assumption of normality, and hence resulting in extremely high or low B-range strength values. A larger sample size is needed to obtain a suitable B-range prediction values.

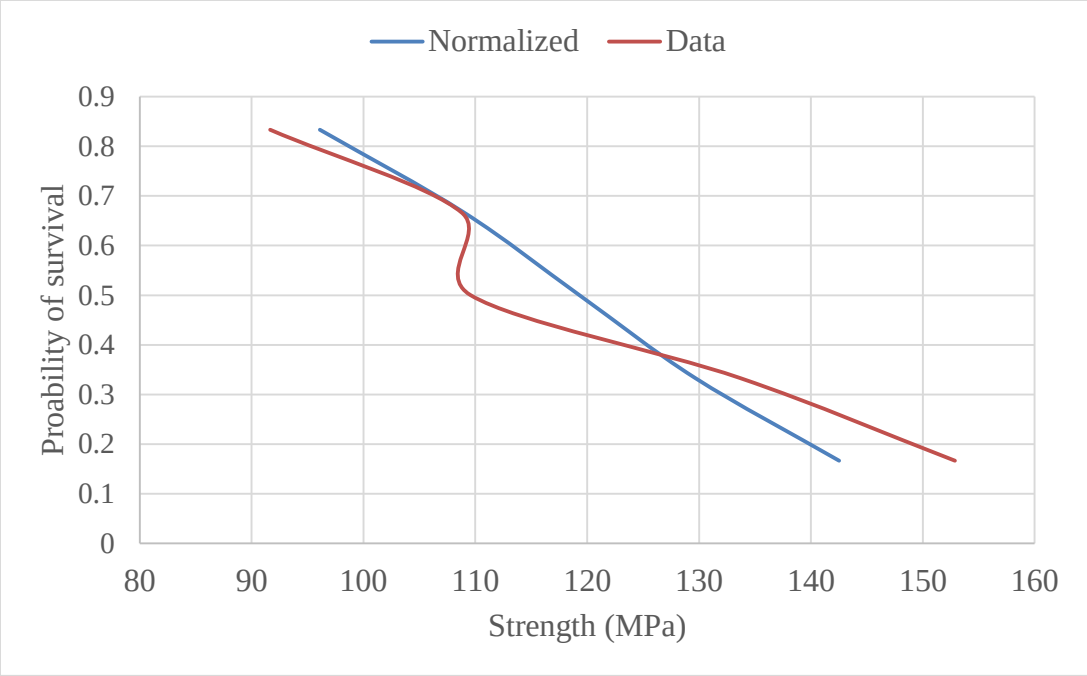

Figure 5.8. Normality distribution of 1.02 mm (0.04 in) thick specimen.

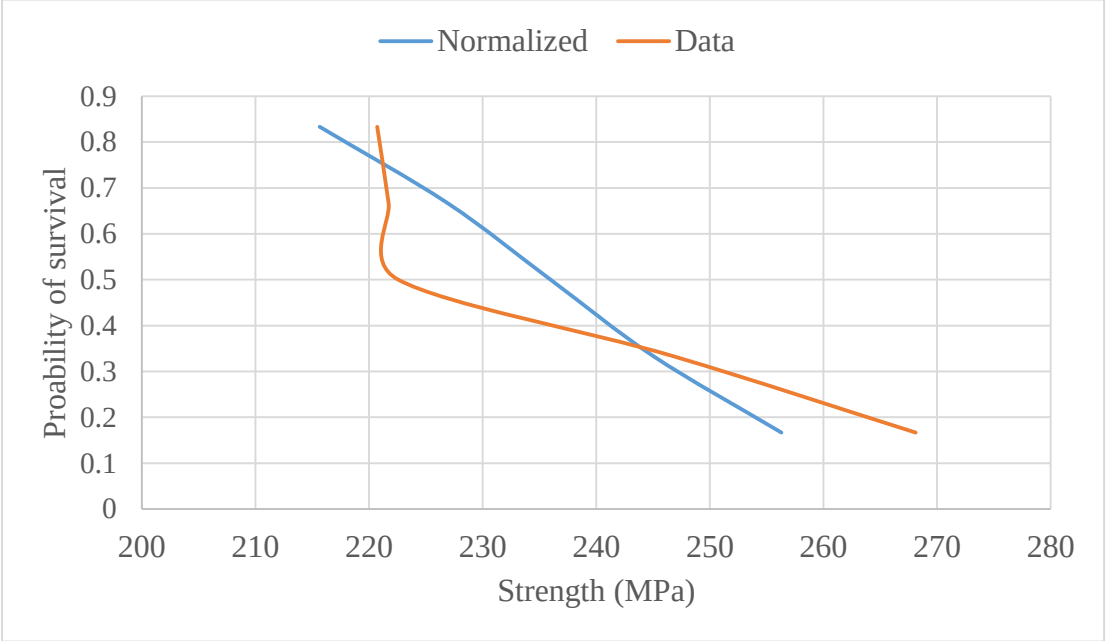

Figure 5.9. Normality distribution of 4.06mm (0.16 in) thick specimen.

5.3.2 *First Structural Failure Criteria of Notched*

The strength results for notched specimens of thickness 2.3mm (0.09 in) with different notch diameters discussed below. The strengths in open hole tension specimens are represented using two approaches, calculating the gross strengths and the net strength. The stress concentration factors in a notched specimen are dependent on the stacking sequence and the stress state near the notch region. The gross and net strengths are shown in equations 5.10 and 5.11. The net strength depends on the presence of the notch in which the load is divided by the cross-sectional area. The gross strength on the other hand, illustrates a load applied at an infinite distance away from the hole, hence the presence of the hole is neglected.

$$\sigma^{\mathrm{Net}} = \frac{\mathrm{P}}{(\mathrm{w}-\mathrm{d})\mathrm{t}} \tag{5.10}$$

$$\sigma^{\mathrm{Gross}} = \frac{\mathrm{P}}{\mathrm{wt}} \tag{5.11}$$

Where:

σ^{Net} = net strength of the specimen

σ^{Gross} = gross strength of the specimen

P = load applied to the specimen

w = width of the specimen, 38.1 mm (1.5 in)

t = thickness of specimen, 2.30 mm (0.09 in)

Table 5.8 to 5.11 summarizes the maximum gross and net strength, computation time and number of chip failure corresponding to each analysis for the different notch diameters tested. For a notch diameter of 6.35 mm (0.125 in), only two analysis were conducted. The gross strength is generally used in the aerospace industry in the generation of allowable strength values

[5]. In this study, the gross strength values will be used to compute the B-basis and B-max strength values for notched specimens.

Table 5.8. Strength Results for Notched Diameter 3.175 mm (0.125 in)

Notch Diameter	Analysis Number	Maximum Gross Strength	Maximum Net Strength	Computation Time (hours)	Number of failed chips
3.175 mm (0.125 in)	1	125.85 MPa (18.26 ksi)	137.29 MPa (19.91 ksi)	21	2000
	2	162.72 MPa (23.60 ksi)	177.51 MPa (25.75 ksi)	28	2021
	3	136.28 MPa (19.77 ksi)	148.67 MPa (21.57 ksi)	28	2047
	4	167 MPa (24.24 ksi)	182.3 MPa (26.44 ksi)	95	14687
	5	148.76 MPa (21.58 ksi)	160.40 MPa (23.26 ksi)	32	2050

Table 5.9. Strength Results for Notch Diameter of 6.35 mm (0.25 in)

Notch Diameter	Analysis Number	Maximum Gross Strength	Maximum Net Strength	Computation Time (hours)	Number of failed chips
6.35 mm (0.25 in)	1	292.30 MPa (42.39 ksi)	350.72 MPa (50.87 ksi)	6.00	308
	2	262.75 MPa (38.11 ksi)	315.30 MPa (45.74 ksi)	2.00	261

Table 5.10. Strength Results for Notch Diameter of 9.53 mm (0.375 in)

Notch Diameter	Analysis Number	Maximum Gross Strength	Maximum Net Strength	Computation Time (hours)	Number of failed chips
9.53 mm (0.375 in)	1	114.35 MPa (16.59 ksi)	152.47 MPa (22.12 ksi)	13.15	2239
	2	139.60 MPa (20.25 ksi)	186.17 MPa (27.00 ksi)	25.13	3633
	3	133.12 MPa (19.31 ksi)	176.33 MPa (25.75 ksi)	34.88	5579
	4	139.05 MPa (20.17 ksi)	185.40 MPa (26.89 ksi)	54.76	8796
	5	137.78 MPa (19.99 ksi)	183.71 MPa (26.65 ksi)	22.98	3590

Table 5.11. Strength Results for Notch Diameter of 12.7 mm (0.50 in)

Notch Diameter	Analysis Number	Maximum Gross Strength	Maximum Net Strength	Computation Time (hours)	Number of failed chips
12.7 mm (0.50 in)	1	94.72 MPa (13.74 ksi)	142.07 MPa (20.61 ksi)	4.24	646
	2	124.18 MPa (18.01 ksi)	186.27 MPa (27.02 ksi)	8.92	1733
	3	115.96 MPa (16.82 ksi)	173.94 MPa (25.23 ksi)	4.52	838
	4	123.13 MPa (17.86 ksi)	184.70 MPa (26.79 ksi)	8.81	1672
	5	156.41 MPa (22.69 ksi)	104.27 MPa (15.13 ksi)	4.20	812

Figures 5.10 to 5.13 show plots of gross strength versus strains for different notch diameters. A common approach used in advanced composite design to compute the strength of notched specimens, is to use the gross-sectional area as it is independent of the geometry. However, for large notch diameters, the use of gross-sectional area in computing the strength could lead to exceedingly over conservative results since the reduction of area is neglected. To compare the predicted results to literature [5], gross-sectional area was used in this study when computing the strength of notched specimens. Figures 5.14 to 5.17 shows the distribution of chip failure for different notch diameter. The results show that as the diameter increases, the chip failure near the notch region, in the net – sectional area increases. For small notch diameters, failure occurred at

the gross regions, away from the notch. Figure 5.18 shows the variation in gross-sectional area strength with respect to the different notch diameters. The gross section versus net section failures were highlighted in the plot in Figure 5.18. The smallest notch diameter, 3.175 mm (0.125 in) had all five elements fail at the net-sectional area. As for the next notch diameter of 6.35 mm (0.25 in), all two of its elements failed away from the notch. For a notch diameter of 9.53 mm (0.375 in), two chips failed at the same element near the notch region, leading to a total of three chip failures near the hole and two chip failure away from the hole. The largest notch diameter 12.7 mm (0.50 in) had three elements fail near or at the notch, while two elements failed in gross-sectional area. Table 5.12 summarizes the B-basis, B-max and average gross strengths for notch diameters of 3.175 mm (0.125 in), 6.53 mm (0.375 in) and 12.7 mm (0.50 in) from the five analysis tested. The B-range values were not computed for a notch diameter of 6.53 mm (0.25 in) since only two analysis were computed. Figure 5.19 shows a bar chart of the B-range and average values.

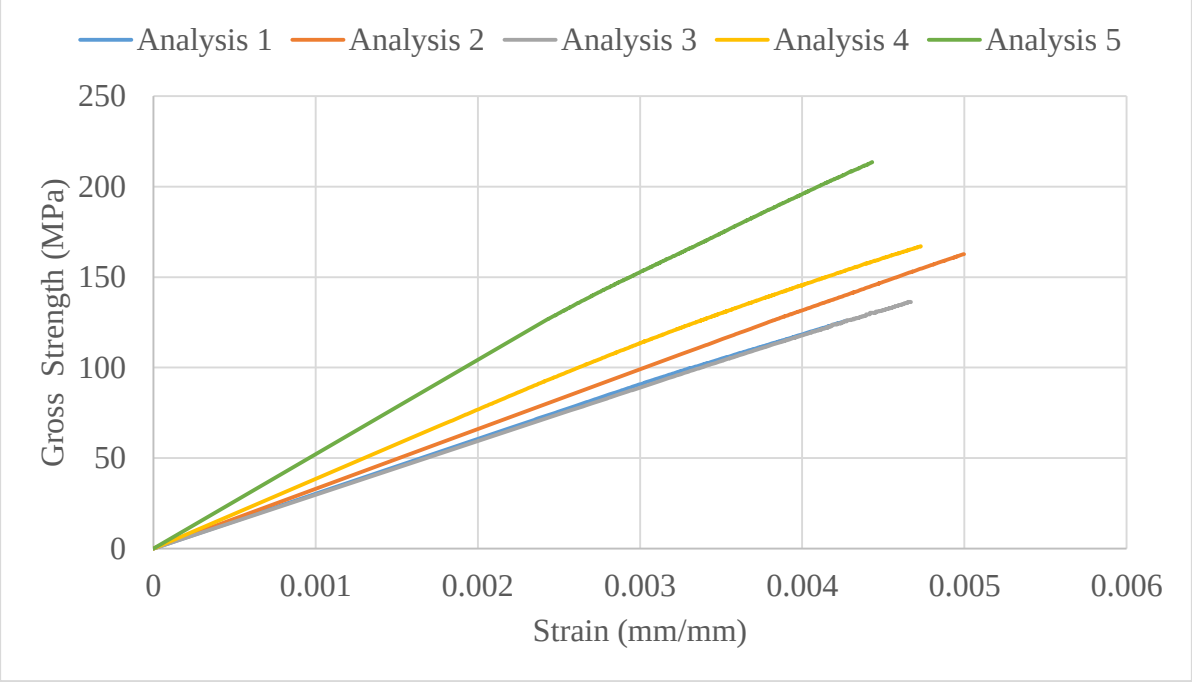

Figure 5.10. Representative gross strength-strain curves for notch diameter of 3.175 mm (0.125in).

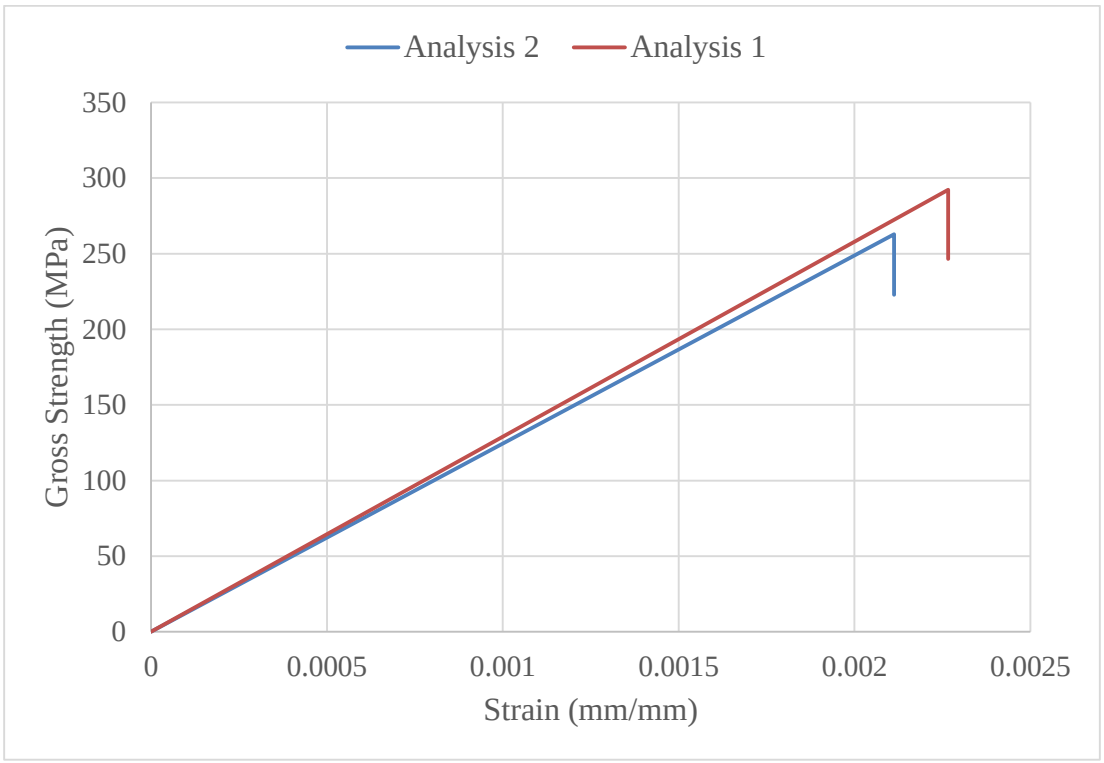

Figure 5.11. Representative gross strength-strain curves for notch hole 6.35 mm (0.25in).

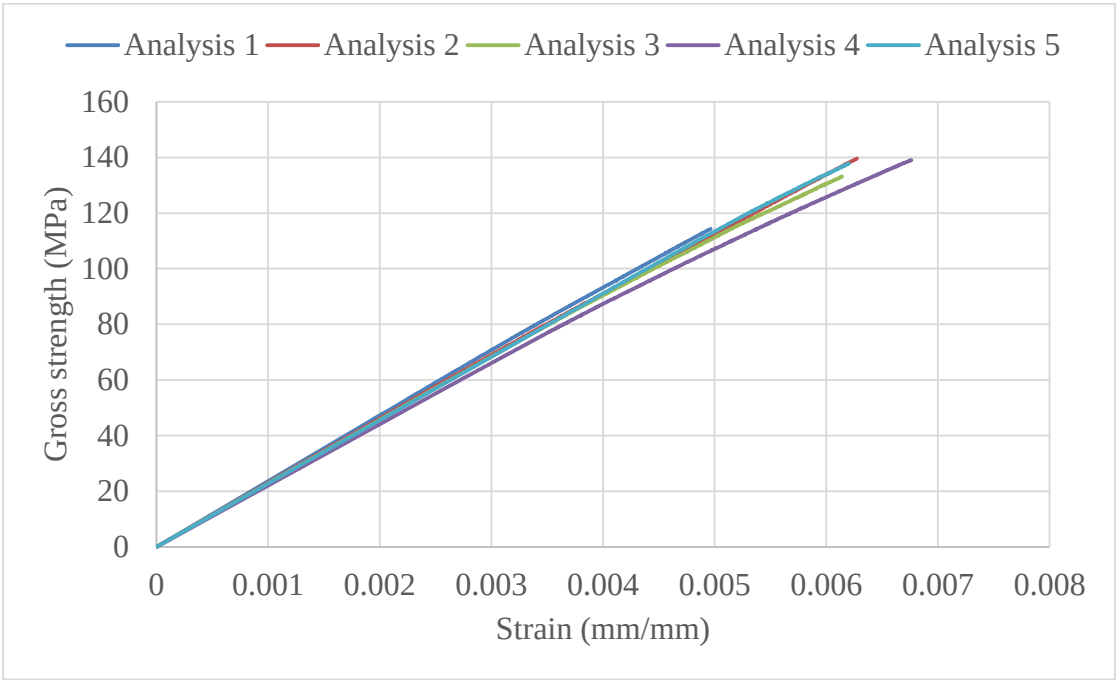

Figure 5.12. Representative gross strength-strain curves for notch hole 9.53 mm (0.375in).

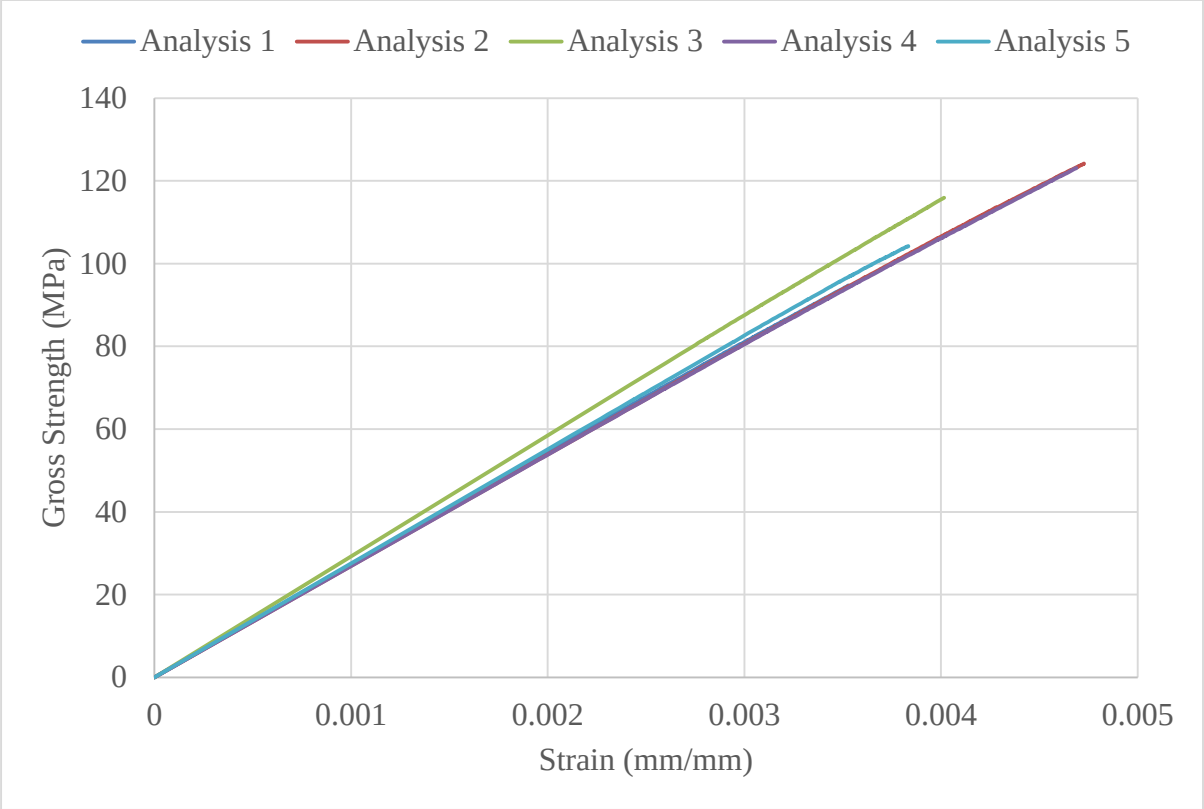

Figure 5.13. Gross strength-strain curves for notch hole 12.7 mm (0.50 in).

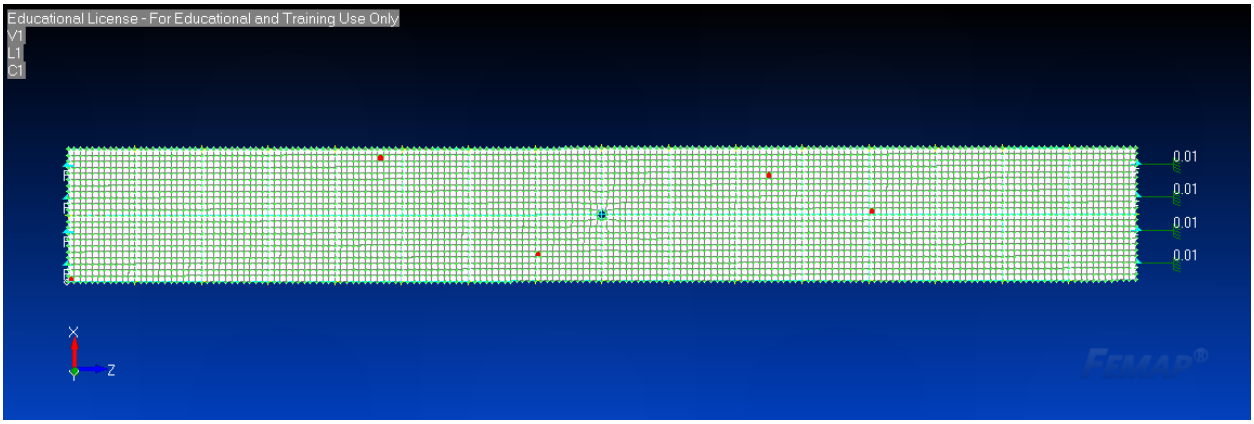

Figure 5.14. Distribution of chip failure for a notch diameter of 3.175 mm (0.125 in).

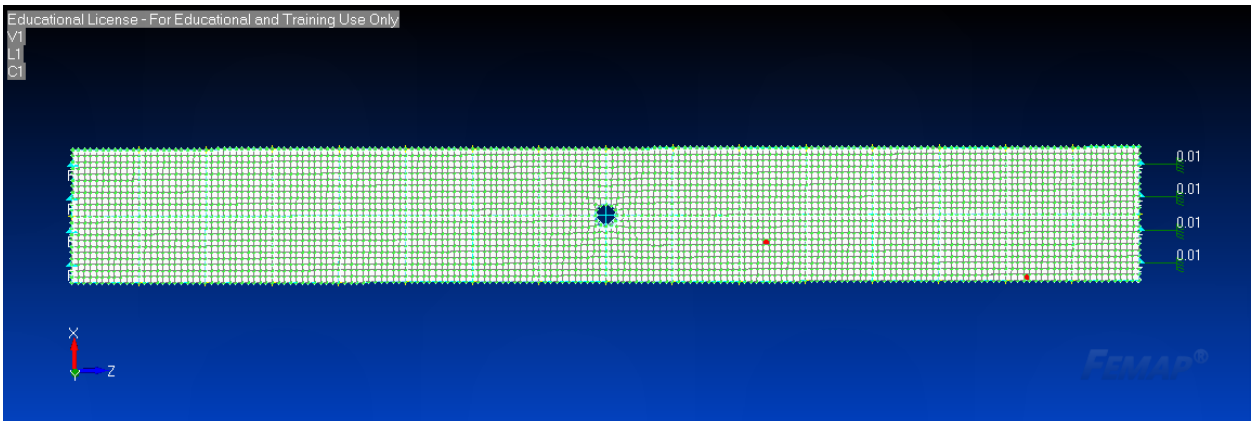

Figure 5.15. Distribution of chip failure for a notch diameter of 6.35 mm (0.25 in).

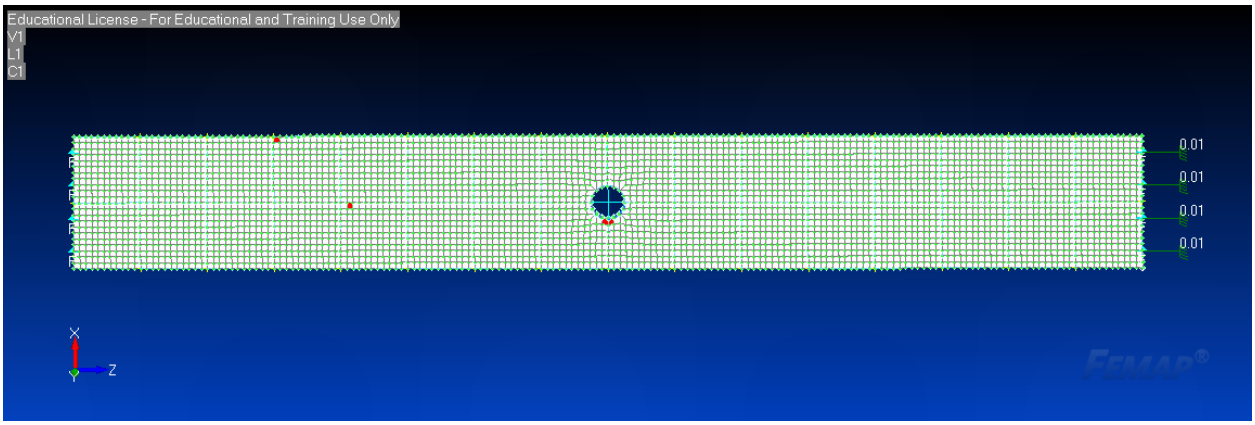

Figure 5.16. Distribution of chip failure for notch diameter of 9.53 mm (0.375 in)

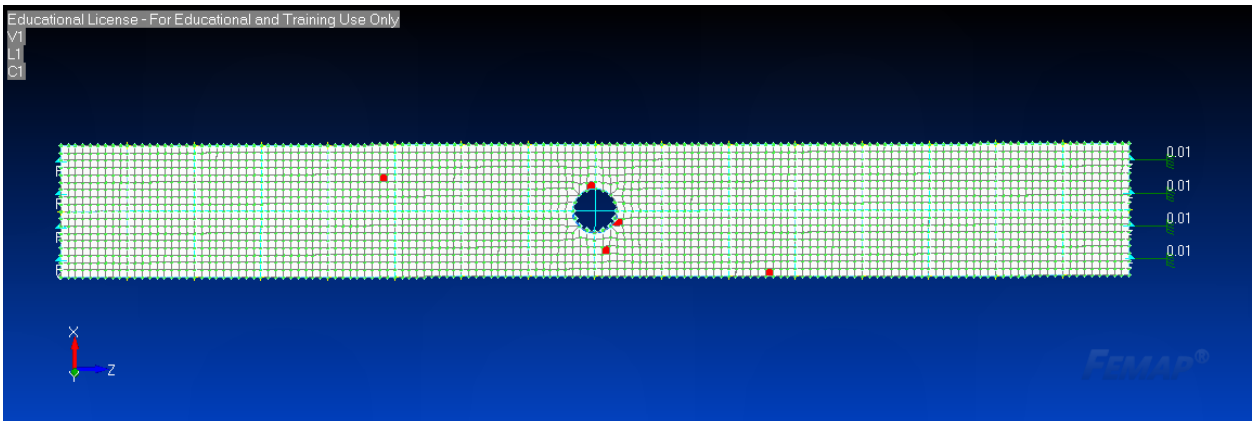

Figure 5.17. Distribution of chip failure for notch diameter of 12.7 mm (0.5 in)

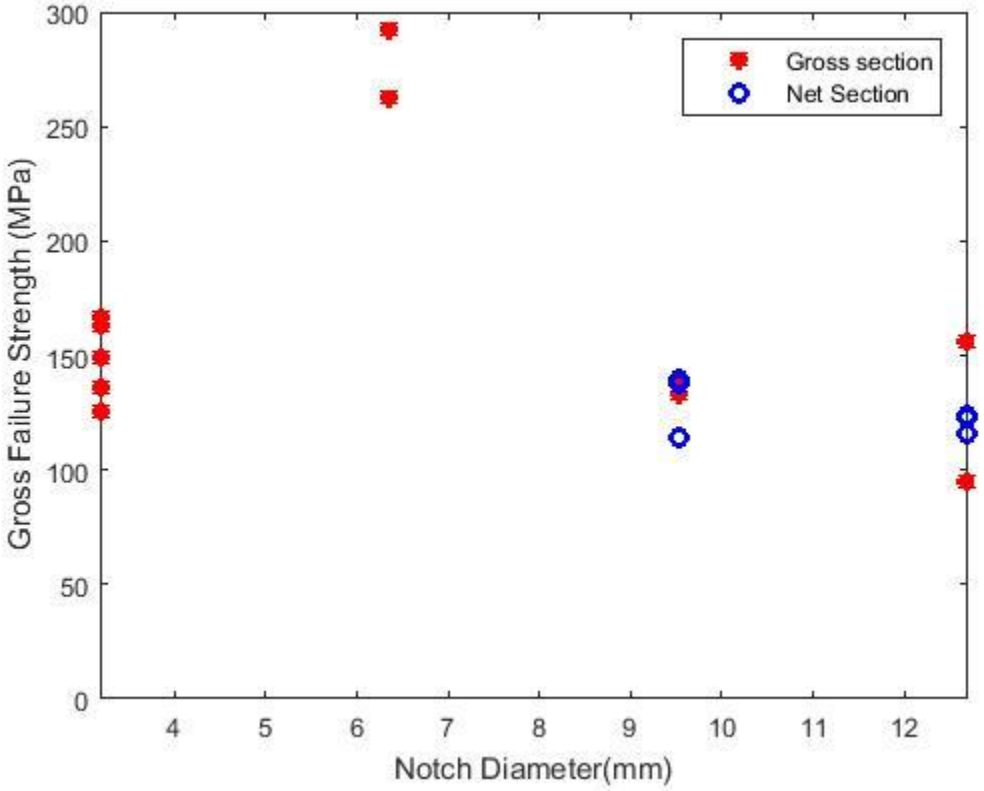

Figure 5.18. Variation of notched strength using gross-sectional area.

Table 5.12. B-max, B-basis and Average values of notched specimens

Notch Diameter	B-basis	Average	B-max
3.175 mm (0.125 in)	76.85 MPa (11.15 ksi)	148.12 MPa (21.48 ksi)	219.39 MPa (31.82 ksi)
9.53 mm (0.375 in)	89.22 MPa (12.94 ksi)	132.78 MPa (19.26 ksi)	176.34 MPa (25.58 ksi)
12.7 mm (0.50 in)	60.33 MPa (8.75 ksi)	112.45 MPa (16.31 ksi)	164.58 MPa (23.87 ksi)

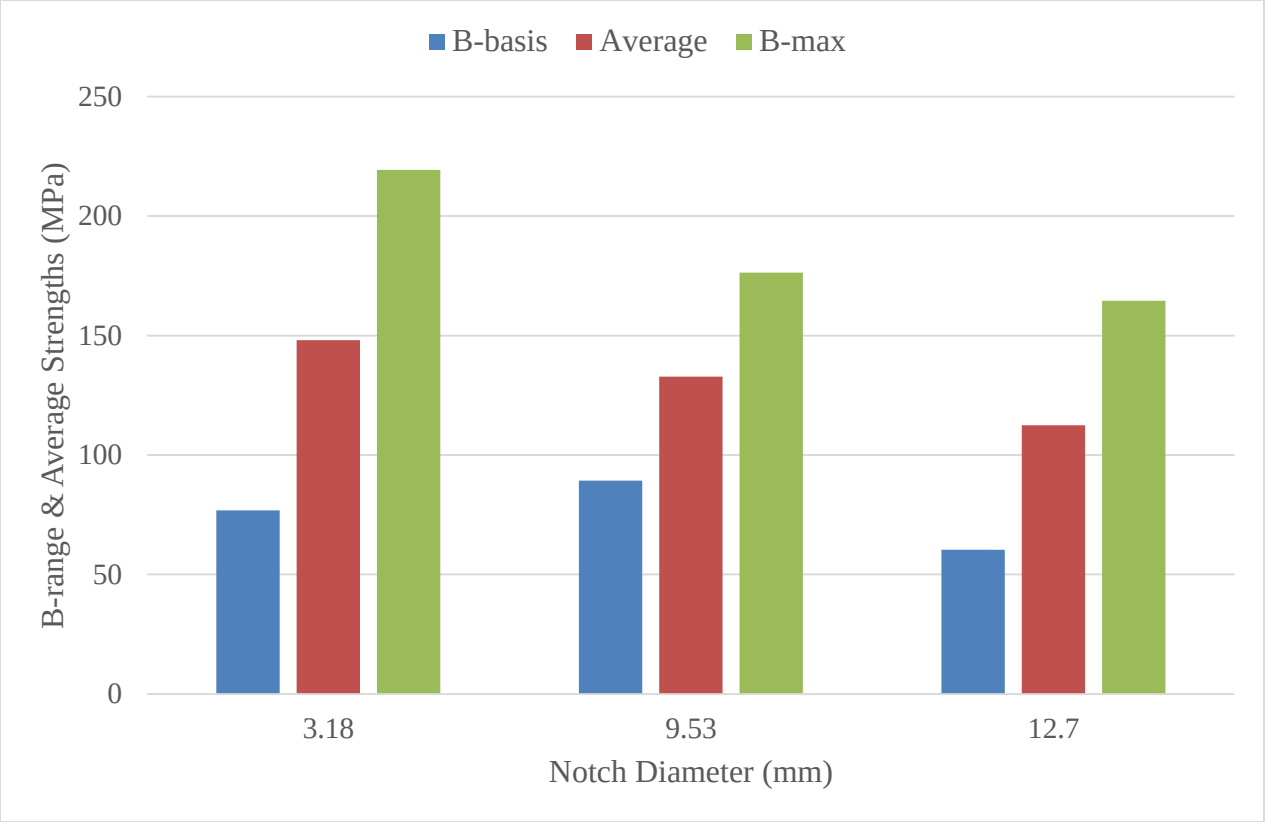

Figure 5.19. B-basis, average and B-max gross strengths for notch diameters.

5.3.3 *Discussion of First Structural Failure*

The first structural failure was adapted to predict the strengths of both the un-notched and notched specimens. Un-notched tension specimens show that chip failure were randomly distributed throughout the specimen, due to the heterogeneous nature of the material. As for the notched specimens, no conclusive trend emerged to suggest that there is a relationship between the notch diameter and the magnitude of strengths. The results show that as the notch diameter increases, more chips fail in the net section, that is close to or at the notch. The uncertainty of failure region of the notched specimens analyzed proves that HexMC materials are notch insensitive. Typically, for homogeneous materials, the presence of a notch would result in localized failure around the notch region, discontinuous fiber composites on the other hand are insensitive to the presence of

notches. This results agree qualitatively with results presented by two literatures [5, 23]. According to Feraboli's test results, the number of specimen that failed in the net section increased as the hole diameter increased. The second literature reported that discontinuous fibers, when compared to continuous fiber composites are not affected by notches [23].

The B-basis, average and B-max gross strength predictions computed for the un-notched and notched specimens could be improved by obtaining a larger sample size. The sample size in this study was significantly low. This was proven by visually plotting the normalized predicted strengths against the predicted strengths, and the normality assumption was disobeyed. Apart from that, the predicted strength values when compared with proprietary Hexcel values [21] reported about 45% to 53% difference. A challenge encountered in running the strength prediction analysis, was that the computation times were extremely long, in which a single analysis could take up to 97 hours to complete. Defining a structural failure criteria that is conservative yet takes a reasonable amount of time to compute is certainly a challenge, but could be a possible focus for future work.

5.3.4 *Second Structural Failure Criteria of Notched*

The second structural failure criteria as described in Section 5.1.2 describes failure when a specified number of chips in the overall specimen has failed. For this second structural failure criteria, the smallest notch diameter was selected to increase the efficiency in terms of computation times. A random number of chips was selected as a basis in which when that number of chips failed, final structural failure is achieved. In this study, a number of 2000 chips and 10,000 chips was used to define this structural failure criteria. Two analysis each was done on the specimen with the smallest notch diameter, 3.175 mm (0.125 in). The results of the analysis at which when 2000 chips failed were summarized in Table 5.13 Both analysis

Table 5.13. Strength values when 2000 chips failed

Analysis Number	Max Gross Strength	Max Net Strength	Instantaneous Slope	Computation Time
1	125.85 MPa (18.26 ksi)	137.29 MPa (19.91 ksi)	52.13 MPa (7.560 ksi)	21 hours
2	146.68 MPa (212.74 ksi)	160.0 MPa (23.21 ksi)	30.30 MPa (4.39 ksi)	23 hours

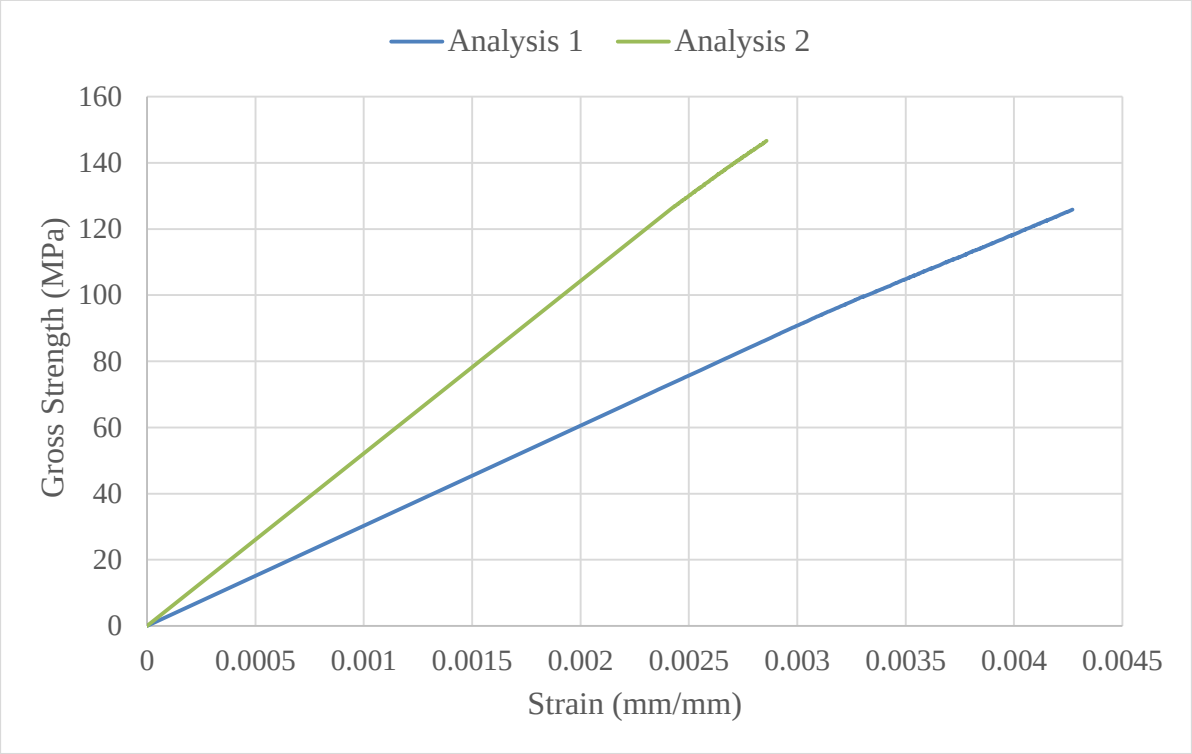

Figure 5.20. Strength-strain curve when 2000 chips fail.

Table 5.14. Strength values when 10,000 chips failed

Analysis Number	Max Gross Strength	Max Net Strength	Gross Area Elastic Moduli	Computation Time
1	203.3 MPa (29.49 ksi)	152.30 MPa (22.10 ksi)	52.13 MPa	90 hours
2	221.78 MPa (32.20 ksi)	166.2 MPa (24.11 ksi)	38.42 MPa	93 hours

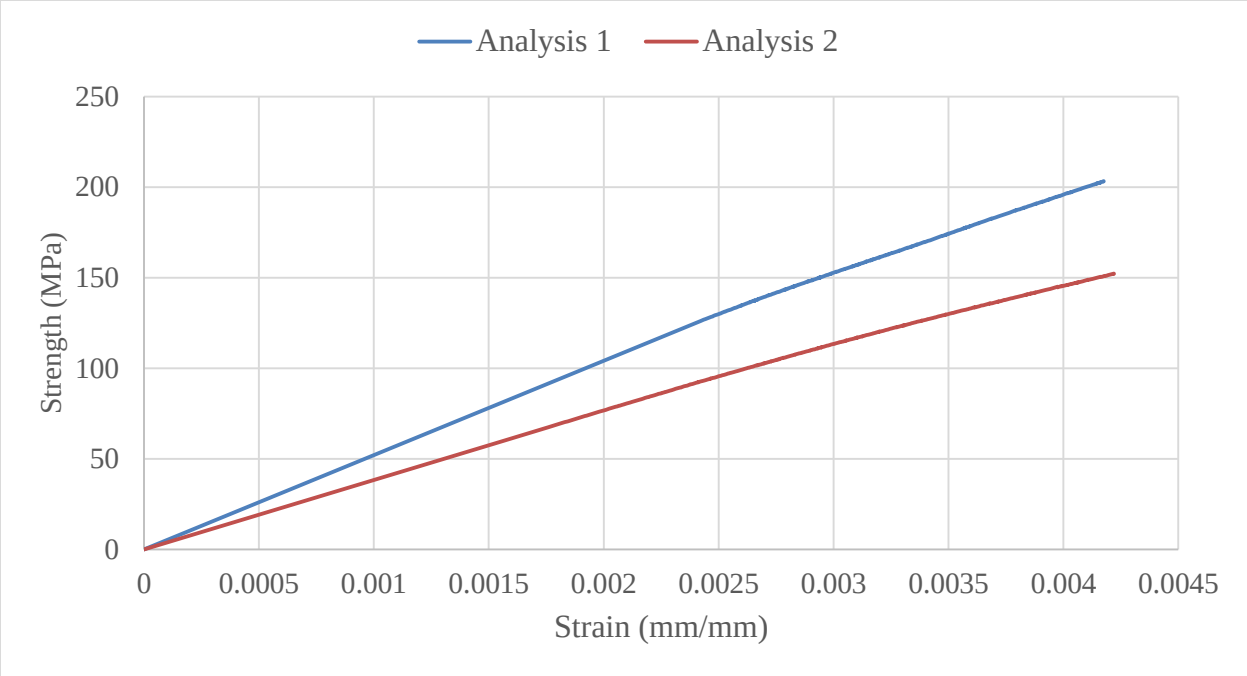

Figure 5.21. Strength-strain curves when 10,000 chips fail.

5.3.5 *Second Structural Failure Discussion*

The second structural failure criteria was arbitrarily defined. Two sub-categories of this failure definition was experimented with, in which failure was reached when 2000 chips failed and when 10,000 chips failed. Due to the non-symmetric and random stacking sequence, the 2000 or 10,000 chips that failed could be anywhere throughout the entire specimen, and does not necessarily imply that a single element has failed. The issue with using this structural failure definition is, that the time taken to reach 10,000 failed chips is extremely long and not practical. Perhaps, a specified number of chip failure could be determined analytically instead of arbitrarily choosing the number of chip failure could be a focus for future work.

Chapter 6. EXPERIMENTAL TESTING

Experimental data was collected from an experiment done at the UW on five HexMC samples. The experiment was done to obtain stress-strain curves at failure to validate the strength results using a damage accumulation model based on the stochastic laminate analogy, as described in Section 5.3.

6.1 MEASURED DIMENSIONS

A total of five HexMC flat panels were tested. Since HexMC's are made out of randomly oriented AS4/8552 graphite epoxy chips, the thickness and the width of the specimen varies longitudinally and transversely. Hence, the width and thickness dimensions were obtained at four different locations, listed in Table 6.1. The average of the width and thickness at the four different locations were obtained and taken to be the nominal dimensions of the specimens. Table 6.2 summarizes the nominal dimensions of the five HexMC flat panels tested.

Table 6.1. Width and thickness dimensions of four different locations

Specimen Number	Location 1		Location 2		Location 3		Location 4	
	Width	Thickness	Width	Thickness	Width	Thickness	Width	Thickness
1	38 mm (1.48 in)	3.80 mm (0.150 in)	38 mm (1.48 in)	3.78 mm (0.148 in)	38 mm (1.48 in)	3.80 mm (0.150 in)	38 mm (1.48 in)	3.84 mm (0.151 in)
2	39.1 mm (1.54 in)	3.80 mm (0.150 in)	39.1 mm (1.54 in)	3.91 mm (0.154 in)	39.3 mm (1.55 in)	3.86 mm (0.152 in)	39.6 mm (1.56 in)	3.89 mm (0.153 in)
3	39.1.mm (1.54 in)	3.86 mm (0.152 in)	39.1 m (1.54 in)	3.86 mm (0.152 in)	39.1 mm (1.54 in)	3.84 mm (0.151 in)	39.1 mm (1.54 in)	3.89 mm (0.153in)
4	38.9 mm (1.53 in)	3.84 mm (0.151 in)	38.9 mm (1.53 in)	3.89 mm (0.153 in)	38.9 mm (1.53 in)	3.86 mm (0.152 in)	38.9 mm (1.53 in)	3.89 mm (0.153 in)
5	39.1 mm (1.54 in)	3.81 mm (0.150 in)	39.1 mm (1.54 in)	3.91 mm (0.154 in)	38.1 mm (1.50 in)	3.94 mm (0.155 in)	39.4 mm (1.55 in)	3.84 mm (0.151 in)

Table 6.2. Nominal width and thickness dimensions

Specimen Number	Width	Thickness
1	37.62 mm (1.481 in)	3.81 mm (0.150 in)
2	39.2 mm (1.545 in)	3.84 mm (0.151 in)
3	39.17 mm (1.542 in)	3.84 mm (0.151 in)
4	38.89 mm (1.531 in)	3.86 mm (0.152 in)
5	39.12 mm (1.540 in)	3.78 mm (0.149 in)

6.2 EXPERIMENT SETUP

The flat panels were loaded in an Instron 5585H frame subjected to a tensile load. About three inches of each end of the flat panels were clamped in the fixture, leaving about an inch and a half of gage length subjected to tensile load. Grit paper was placed in between the specimen and the frame grips to ensure a better grip of the HexMC flat panels. A knife edge was attached to the gage area of the specimen to measure the corresponding strains. Figure 6.1 shows a HexMC flat panel mounted in the test fixture, being loaded by the Instron test frame.

Figure 6.1. Experimental Setup using Instron 5585H

6.3 EXPERIMENTAL RESULTS

Five HexMC flat panels were tested and loaded on the Instron until fracture. The fracture load recorded was about 300 MPa (43.5 ksi) to 400 MPa (58 ksi). For this experiment, fracture was recorded when the flat panels were divided into two separate pieces. Figure 6.2 shows fracture regions of the five HexMC flat panels in order. Fracture region was mostly seen closer to the bottom end of the specimen, only one specimen recorded a fracture region closer to the top end. After all the tests were completed, the strain measurements were corrected for slipping of the

grips. The slipping occurred due to the friction between the grit paper and the testing grip. As a result of this grip slipping, nonlinearity was seen in the plots, hence the strains were corrected. The stress versus strain plots shown in Figure 6.3 has the same trend as the strength versus strain plots for the notched and un-notched panels in Section 5.3.1. The plots of stress versus strain in Figure 6.3 is close to linearity with the exception of some minor slipping during the testing.

Figure 6.2. Fracture regions of HexMC Flat Panels

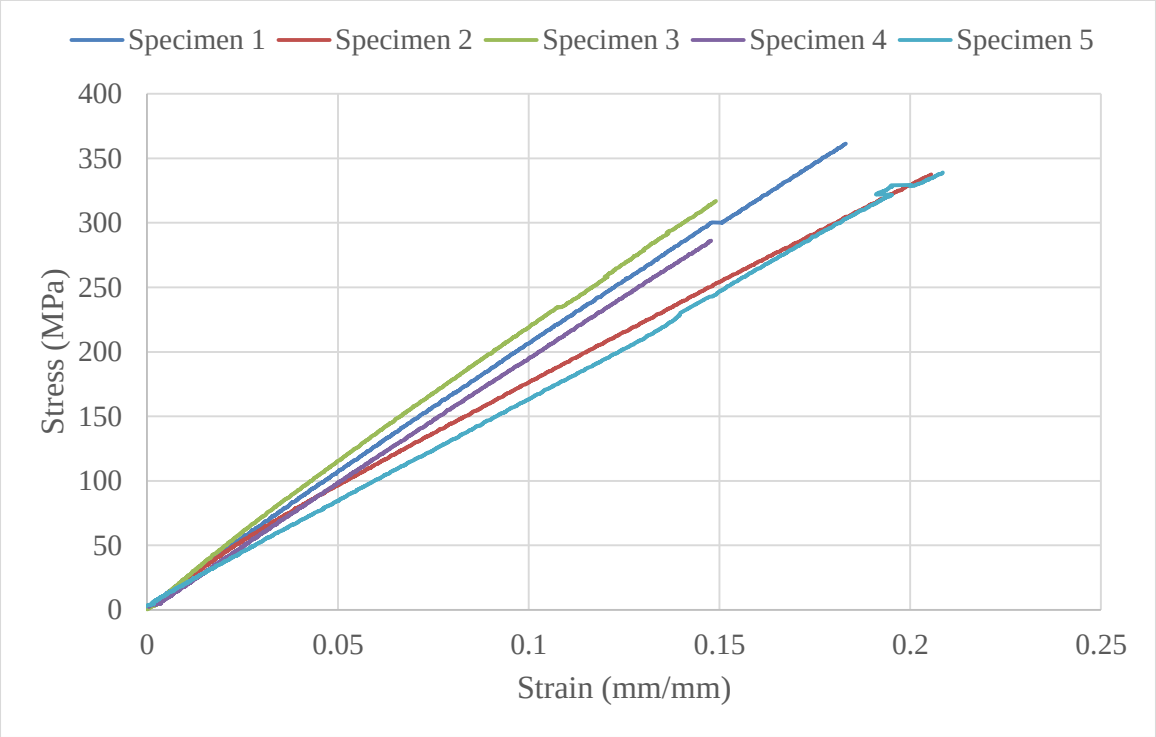

Figure 6.3. Stress versus strain for five HexMC flat panels

6.4 Improvement Of Predictions

In order to improve the accuracy of the HexMC testing, several factors should be considered and further addressed. To more accurately predict the fracture of the HexMC flat panels, the specimens should be properly gripped and held firmly by the Instron grips. Since HexMCs are made out of randomly oriented chips, the thickness of the throughout the entire specimen is not uniform. In this study, the nominal thickness was obtained by averaging the thickness measurements at four different locations, this variation in measurements could lead to inaccurate nominal dimensions.

Another factor that could influence the accuracy of reading is the presence of localized failure, prior to failure or the onset of loading. During testing, audible cracks were heard before fracture occurred. Ensuring the specimen tested have no localized failure could be a focus for future work. Lastly, the disparity between measurements and predictions is probably due to the misalignment during the test set-up, the material properties of HexMC versus the reduced material properties used in the simulation.

Chapter 7. CONCLUSION

The goal of this study was to develop a numerical modeling approach that predicts the B-basis and B-max stiffness and strength that will ultimately lead to the certification of discontinuous fiber composites based on analysis. The principal results of this study are summarized and described in the preceding paragraph.

- The B-basis and B-max stiffness was successfully predicted by 150 randomly generated random layup volume elements which is equivalent to 150 number of samples. The B-max and B-basis stiffness should be calculated using a reasonably large sample size to obtain a normal distribution. The B-basis stiffness was calculated following a procedure similar t that used for the calculations of B-basis strengths. The B-max stiffness on the other hand, was calculated using a similar procedure with slight modifications to account for the stiffness under which 90% of the predicted stiffness should fall 95% of the time.
- The B-basis and B-max strengths was predicted using a damage accumulation model called the ply discount scheme based on the stochastic laminate analogy. This process was hindered by extremely long computation times, ranging from about 8 – 95 hours for a single analysis. Several final structural failure criteria was experimented with the limitation of the number of analysis conducted due to computation expenses. Desirably, the number of analysis required to obtain a good prediction of B-basis and B-max strengths should be more than 5, and closer to 150 as done for the stiffness predictions.

The challenges faced in this study was the identification of an appropriate final structural failure criteria and the computational expenses involved.

Chapter 8. FUTURE WORK

Overall, this study was successful in predicting the B-basis and B-max stiffness. The limitations of this study in predicting the strengths, as discussed results from the long computation times. Additionally, more analysis should be done to obtain a better prediction of the B-range values. Two final structural failure criteria's were experimented with in this study, with a heavy focus on the first final structural failure criteria to account for less computation times. Applying a final structural failure criteria that is conservative yet consumes a reasonable amount of time certainly is a challenge, but would be worth looking into for future work. Several other consideration of final structural failure criteria has been suggested, which include defining failure when the instantaneous slope of the stress-strain curve has been reduced by some specified amount or when all chips within the structure have failed. The use of high-performance cluster to minimize computational time is currently being investigated.

REFERENCES

[1] Boeing, “Boeing 787 from the Ground Up” [Online]. Available: http://www.boeing.com/commercial/aeromagazine/articles/qtr_4_06/article_04_2.html. [Accessed 9 Nov 2013]

[2] Boeing, “Boeing 7E7 Structure Will Be Made of Composite Materials” [Online]. Available: http://boeing.mediaroom.com/2003-06-12-Boeing-7E7-Structure-Will-Be-Made-of-Composite-Materials. [Accessed 9 Nov 2013].

[3] J. C. Halpin, “Stiffness and Expansion Estimates for Oriented Short Fiber Composites,” *Journal of Composite Materials,* vol.3, no. October, pp. 732-734, 1969.

[4] P. Feraboli, E. Peitso, T. Cleveland and P. B. Stickler, “Modulus Measurement for Prepreg-based Discontinues Carbon Fiber/Epoxy Systems,” *Journal of Composite Materials,* vol. 43, no. 19, pp. 1947-1965, 2009.

[5] P. Feraboli, E. Peitso, T. Cleveland and P. B. Stickler, “Notched behavior of prepreg-based discontinues carbon fiber/epoxy systems,” *Composites: Part A,* vol. 40, no. 3, pp. 289-299, 2009.

[6] The Hexcel Corporation, “AMTAS Test Report Allowable for HexMC Materials, Document No. HSTR 00006,” The Hexcel Corporation, 2010.

[7] P. Feraboli, T. Cleveland, P. Stickler and J. Hapin, “Stochastic laminate analogy for simulating the variability in modulus of discontinuous composite materials,” *Composite: Part A,* vol. 41, no. 4, pp. 557-570, 2010.

[8] J.C. Halpin and N. J. Pagano, “The Laminate Approximation for Randomly Oriented Fiber Composites,” *Journal of Composite Materials,* vol. 3, pp. 720, 1969.

[9] Head, B., and Tuttle, M., Analysis Methods for Discontinuous Fiber Composites, Seattle: University of Washington, 2013.

[10] “Custom Formulated Bulk & Sheet Molding Compounds,” Composites International, [Online]. Available: http://www.idicomposites.com/smc-bmc.php. [Accessed 28 November 2015].

[11] P. Feraboli, E. Peitso, F. Deleo, T. Cleveland, M. Graves and P. Stickler, “Characterization of Discontinuous Carbon Fiber/Epoxy Systems for Aerospace Applications: Part I,” *Journal of Reinforced Plastic and Composites,* vol. 28, no 10, pp. 1911-1915, 2009.

[12] Head, B., and Tuttle, M., "Certification of Discontinuous Fiber Composite Forms for Aircraft Structures", Proceedings, JAMS 2013 Technical Review, Wichita, KS, www.niar.wichita.edu/coe/cecam/Certification_of_Discontinuous_Fiber_Composite_Forms for_Aircraft_Structures-Tuttle.pdf , 2013.

[13] Siemens PLM Software, "NX Nastran 10 Help Library," 2015. [Online]. [Accessed 14 November 2015].

[14] Marlett, K., "Hexcel 8552 AS4 Unidirectional Materials Property Data Report", Nov 2011. Available online at: http://www.niar.wichita.edu/coe/ncamphexcel.asp

[15] McGowan, D.M., and Ambur, D. R., "Damage Characteristics and Residual Strength of Composite Sandwich Panels Impacted With And Without Compression Loading", 39thAIAA/ASME/ASCE/AHS/ASC SSDMC Conference (AIAA Paper No. 98-1783), Long Beach, CA (1998).

[16] U.S. Department of Defense, "Statistical Methods," in *Military Handbook Vol. 8: Polymer Matrix Composites Guidelines for Characterization of Structural Materials*, p. Volume 1 Ch. 8.

[17] Bogucki, G., Bayldon, J., Gintert, L., Ward, S., McCarvill,W., and Tomblin J., Material Qualification and Equivalency for Polymer Matrix Composite Material Systems: Updated Procedure", Report No DOT/FAA/AR-03/19, May 2007.

[18] Shyprykevich, P., "The Role of Statistical Data Reduction in the Development of Design Allowables for Composites," Test Methods for Design Allowables for Fibrous Composites: 2nd Volume, ASTM STP 1003, C.C. Chamis, ed., American Society for Testing and Materials, Philadelphia, PA, 1989, pp. 111-135.

[19] Montgomery, Douglas C., George C. Runger, and Norma Faris Hubele. "Random Variables and Probability Distribution." *Engineering Statistics*. New York: John Wiley, 2001. 80-84. Print.

[20] Tuttle, Mark. "Unidirectional Composite Laminates Subject to Plane Stress."*Structural Analysis of Polymeric Composite Materials,*" 2nd ed. S.l.: CRC, 2012. 229-33. Print.

[21] Hexcel Product Data Sheet: http://w ww.hexcel.com/Resources/DataSheets/Prepreg-Data-Sheets/8552_eu.pdf

[22] C.Qian, L.T Harper*, T.A. Turner, N.A. Warrior, "Notched behavior of discontinuous carbon fibre composites: Comparison with quasi-isotropic non-crimp fabric," *Composites: Part A*, vol. 42, pp. 293-295, 2011.

[23] Bruno Boursier, Alfonso Lopex, "Failure Initiation and Effect of Defects in Structural Discontinous Fiber Composites," Society for Advancement of Material and Process Engineering, Dublin, Ca, 2010.